Using Multiple Layers and Surface Roughness Control for Improving the Sensitivity of SPR Sensors

by

MENG PAN

A thesis submitted to

The University of Birmingham

for the degree of

MASTER OF PHILOSOPHY

School of Mechanical Engineering

College of Engineering and Physical Sciences

The University of Birmingham

December 2009

ABSTRACT

Surface plasmon resonance (SPR) sensors have been developed quickly in the past twenty years in biosensing. However, the sensitivity of them restricts them from small molecular detection. This thesis focuses on the sensor chips of the SPR sensors and presents two potential methods to improve the sensitivity of currently used SPR sensor chips: the bimetallic layer sensor chip and surface roughness control of glass slide. The bimetallic layer sensor chip has been proved to produce better sensitivity performance than the currently used mono gold layer sensor chip by simulation because it takes the advantage of the good sensitivity performance that silver produces and protects silver from oxidizing by the outer gold layer. The surface of the glass slide, as a part of SPR sensor chip, is assumed to be planar in all the current research of SPR biosensors, which is not possible in real case. The surface roughness effect of the glass slide on the sensitivity of SPR sensor chip is investigated. Simulation has suggested that the improvement in the surface roughness of glass slide can enhance the sensitivity performance of SPR sensor chip. By controlling the surface roughness condition of glass slide through polishing, experiments shows that the sensitivity of SPR sensor chips is improved by making the surface of the glass slide smooth.

ACKNOWLEDGEMENTS

Firstly, I would like to express my sincere thank and respect to my supervisor, Dr. Kyle Jiang who provided me with guidance and support during my M. Phil research project. He let me know how to conduct the research project step by step and encourage me to be creative during my study. I would also like to show my appreciation to Dr. Xianzhong Chen for his important suggestions and valuable discussions between us.

I would like to thank Prof. Phil Prewett and Dr. Michael Ward in the micro-engineering group for their suggestions and encouragement towards my study. My special thanks to Dr. James Bowen in Chemical Engineering department for his assistance in the roughness measuring process. I would also like to thank Dr. Mike Keeble from Buehler Laboratory for his help during the glass polishing process. I am appreciated that Mr. Alan Saywell made me the sample holder for the glass polishing.

The assistance and support of all my colleagues in micro-engineering group in my daily research are also very much appreciated. A very big thank to all my friends who accompany me during my research.

Last but no at least, I would like to thank beloved my parents, Haiming Cao and Zheng Pan, who have always been my biggest supporter during my life. They support me continuously with their love and thoughtful concern so that I can finish my research.

CONTENTS

List of Figures

List of Tables

List of Refereed Publications

1. X. Chen, M. Pan, K. Jiang, 'Simulation of the surface roughness effect on the performance of SPR in the Kretschmann configuration', *nanoMan 2008, 13-16, July, 2008, Singapore.*

2. X. Chen, M. Pan, K. Jiang, 'Sensitivity enhancement of SPR biosensor by improving surface quality of glass slides', *MNE09, 28 Sep-1 Oct, 2009, Ghent, Belgium.*

3. X. Chen, M. Pan, K. Jiang, 'Sensitivity enhancement of SPR biosensor by improving surface quality of glass slides', *In Press, Microelectronics Engineering, 2009*

1. INTRODUCTION

1.1 Introduction to SPR Technology

Surface plasmon resonance (SPR) is regarded as one of the most powerful and widely used method applied in current biosensor with its capability in sensitively biomolecular detection.

The physical phenomenon of surface plasmon resonance was first discovered by Wood in 1902 by finding an abnormal diffraction when he shone polarized light onto a mirror with diffraction gratings on the surface [1, 2]. The principle of the phenomenon was first introduced by Fano in 1941 [3]. In 1968, Otto [4], and almost in the same time, Kretschmann and Raether [5] initiate the way to excite surface Plasmon, which formed a complete explanation of surface plasmon resonance. Application of SPR based sensors as biosensors in biomolecular interaction detecting was initially reported by Liedberg in 1982 [6, 7]. After that, SPR technique has experienced long-term development and the first commercially designed SPR biosensor was released in 1990 by BIACore, the world leading biosensor producer based in Sweden.

The features of no-labeling, real time and highly sensitivity enables SPR biosensors a remarkable future in the application of biological detecting, clinical diagnostics, food analysis, etc.

1.2 Aim and Objectives

The aim of the project is to improve the sensitivity of the SPR sensors by developing bimetallic layer SPR sensors and investigating the effect of surface roughness on the sensitivity of the SPR sensor chips. Computer simulation indicates that bimetallic layer SPR sensors can improve the sensitivity considerably. Also, SPR sensor surfaces are assumed as perfectly smooth in simulation but the fabrication process can not produce that quality. It is important to understand how much the surface roughness will affect the sensitivity before a design from simulation can be adopted. It is understood that the sensitivity of SPR sensor is related to various elements, including the optical unit, the data analyzing unit and the sensor surface. In this research, the other parameters of the SPR system remain the same, while the research is focused on the variation of sensor surface roughness and the corresponding performance of the SPR system. Through this way, the effect of the sensor surface roughness on the sensitivity can be found.

The following objectives are identified for implementation to achieve the aims of the research project:

1. To conduct a good literature review of the surface plasmon resonance technology.

2. To discuss the current research projects concerning the sensitivity of SPR

sensor chips.

3. To investigate the improvement in sensitivity of SPR sensor made by multi-layer SPR sensor chips.

4. To evaluate the sensor chip surface roughness effect on the sensitivity of SPR sensor by computational simulation and experiments.

5. To compare the computational results with experimental ones.

1.3 Thesis Overview

The thesis comprises six chapters. The first chapter presents a brief introduction of the SPR technology and indentifies the project aims and objectives. In the second chapter, a complete literature review of the background of SPR biosensors is conducted. Furthermore, the current research background of the sensitivity performance of SPR sensors is presented, thus the project objectives are clarified. In chapter 3, computational method is introduced to analyze the improvements in the sensitivity that the bimetallic layer sensor chip can bring. Chapter 4 presents the simulation results to show how the surface roughness of glass slide can affect the sensitivity of SPR sensor chips. In chapter 5, experiments of glass slides with different roughness condition are introduced to find out the effect of the surface roughness of glass slide on the sensitivity of SPR sensor chips. The experimental results are compared with computational ones to draw conclusions. The study is concluded in chapter 6 where main findings are emphasized and some future work is suggested.

2. LITERATURE REVIEW

2.1 Introduction

In this chapter, a comprehensive literature review of the SPR technology, its applications in biosensing and the current research background of the sensitivity of SPR biosensors are presented. As a cutting-edge technology applied in biosensing, SPR technology has developed fast in the past twenty years and has been studied by researchers in different aspects, including the principle [4, 5, 8, 9], applications [6, 7, 9-11], the enhancement of its current performance [12-21] and new types of SPR biosensors [22-30]. The literature review covers information of surface plasmon resonance coming from various resources, i.e. books, journals and internet databases. It starts from backgrounds SPR technology, the applications of SPR technology, to the existing research that carried out in the sensitivity of SPR sensor chips, and finally, the research objectives of the project.

2.2 Physical Principle of SPR

2.2.1 Introduction

The physical principle of the surface plasmon resonance technology is described in this section. Surface plasmon resonance happens when the wave vector of the

surface plasmons at the interface between dielectric and metal meets the wave vector of the propagating evanescent wave at the interface which is generated by the total internal reflection. There are two important concepts that help to understand the physics of surface plasmon resonance: surface plasmon (SP) [31-33] and the evanescent wave [34].

2.2.2 Surface Plasmons (SPs)

According to Maxwell equation [35], surface plasmon is defined as propagating electron density waves at the interface between dielectric and metal. It happens when free electrons exist at the interface of metal and dielectric material [31] (Figure 2.1).
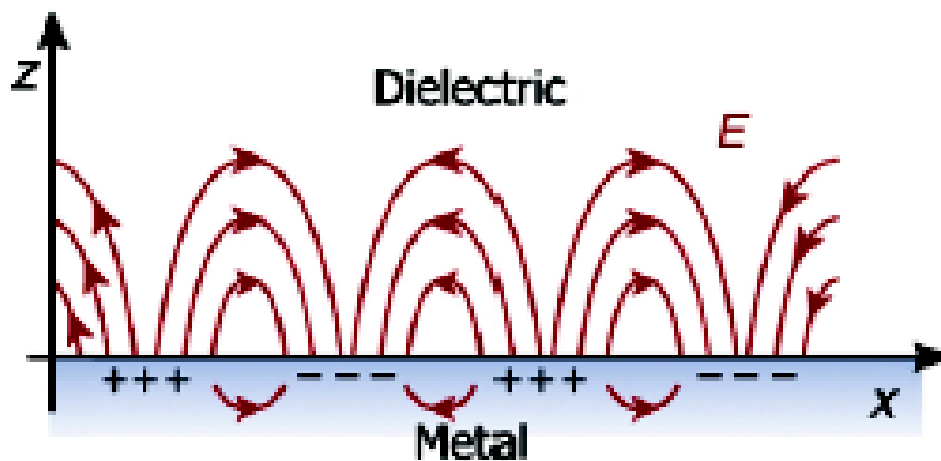
Figure 2.1 Surface plasmons at the interface

2.2.3 The Evanescent Wave

To help demonstrate the evanescent wave, the concept of total internal reflection is introduced at first. Total reflection happens when light goes through from a media with high refractive index to another with a low refractive index. According to Snell's Law [33, 36], when light passes between two media 1 and 2, (Figure 2.2), with refractive indices n_1 and n_2, where $n_1 > n_2$, there is a relationship:

$$n_1 \sin \alpha = n_2 \sin \beta \qquad\qquad (2.1)$$
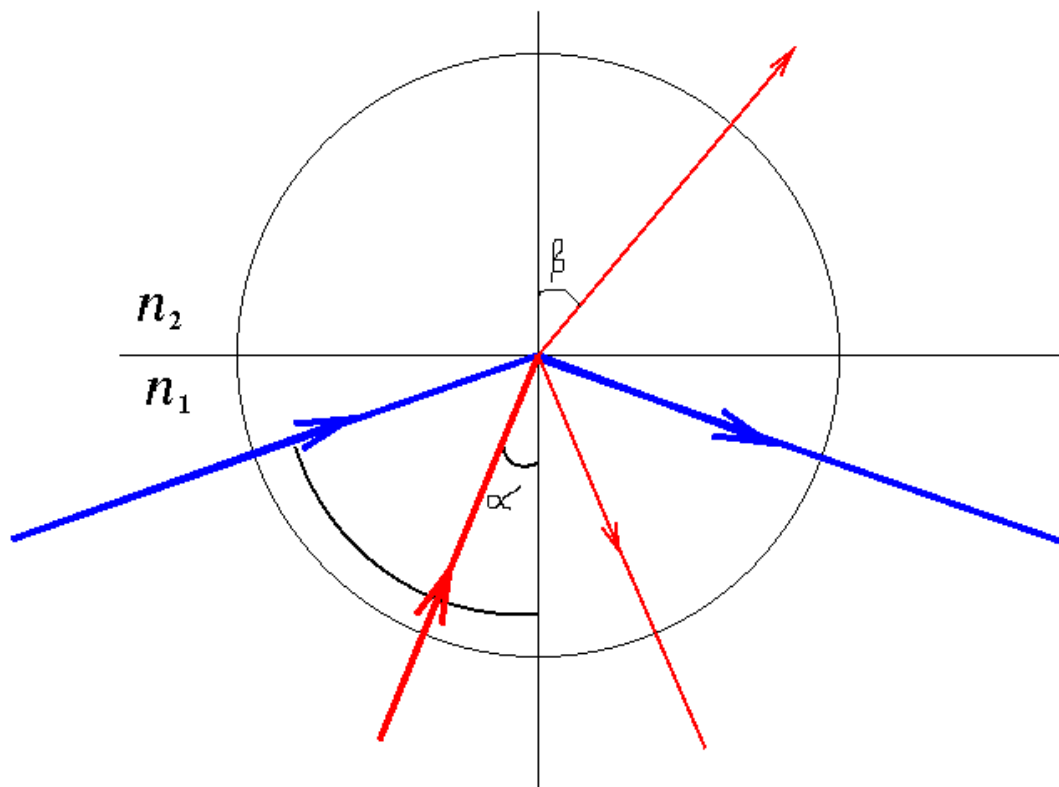
Figure 2.2 Total reflection

When the total reflection happens, no refraction happens, therefore, $\beta = 90°$, and $\sin \beta = 1$.

In this case, $\alpha = \arcsin(\frac{n_2}{n_1})$ is defined as the critical angle. When the incident angle is larger than the critical angle ($\alpha > \arcsin(\frac{n_2}{n_1})$), the total reflection happens.

When a p-polarized incident light travels on the interface between media 1 and 2 (Figure 2.3), the electric fields of the incident, reflected and transmitted light (respectively $\mathbf{E}_i$, $\mathbf{E}_r$ and $\mathbf{E}_t$) are described by

$$\mathbf{E}_i = \mathbf{E}_{ip} \exp i(\mathbf{k}_i \cdot \mathbf{r} - \omega t) \quad (2.2)$$

$$\mathbf{E}_r = \mathbf{E}_{rp} \exp i(\mathbf{k}_r \cdot \mathbf{r} - \omega t) \quad (2.3)$$

$$\mathbf{E}_t = \mathbf{E}_{tp} \exp i(\mathbf{k}_t \cdot \mathbf{r} - \omega t) \quad (2.4),$$

where $\mathbf{E}_{ip}$, $\mathbf{E}_{rp}$ and $\mathbf{E}_{tp}$ are the p-polarized component of them. $\mathbf{k}_i$, $\mathbf{k}_r$ and $\mathbf{k}_t$ are the wavevector of the incident, reflected and transmitted light.

When the total reflectance happens, the angle of incidence (α) is equal to the angle of reflectance.

According to Eq. 2.1, the reflection coefficient for the p-polarized light is:

$$\frac{E_{rp}}{E_{ip}} = r_p = \frac{n_2 \cos \alpha - n_1 \cos \beta}{n_2 \cos \alpha + n_2 \cos \beta} = \frac{\tan(\alpha - \beta)}{\tan(\alpha + \beta)} \quad (2.5)$$

The reflected intensity for the p-polarized light is $R_p = |r_p|^2$ (2.6).

To physically discuss the existence of the evanescent wave, the wavevector **k** (Figure

2.3) is introduced. Its magnitude is

$$k = \sqrt{k_x^2 + k_y^2 + k_z^2} = n\frac{\omega}{c} = n\frac{2\pi}{\lambda} \qquad (2.7),$$

where c is the velocity of propagation and λ is the wavelength.
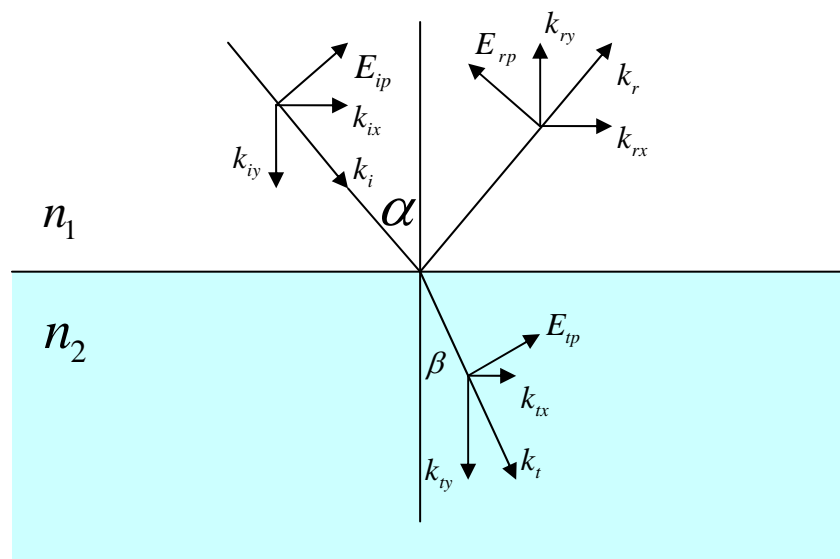
Figure 2.3 Electromagnetic fileds and wavevectors in two media

Light wave at the interface of these two media is discussed in a 2-D condition where

$k_z = 0$. From Eq. 2.1, the wavevector along X axis is

$$k_{ix} = k_{tx} = k_x \qquad (2.8).$$

By substituting Eq. 2.8 into Eq 2.7, an expression for k_{ty} can be obtained

$$k_{ty} = n_1 \left(\frac{2\pi}{\lambda}\right)\sqrt{\frac{n_2^2}{n_1^2} - \sin^2 \alpha} \qquad (2.9)$$

, and it is perpendicular to the interface.

Now, when the total internal reflection happens, it holds that $\sin\alpha > \dfrac{n_2}{n_1}$ as

mentioned before. As a result, k_{ty} is imaginary, representing that the light wave

perpendicular to the interface does not exist. Therefore, the transmitted light wave

propagates parallel to the interface in the media with the lower refractive index for the

depth nearly about the same as the wavelength of the incident light. Additionally, it

propagates at the interface of these two medium for about half the wavelength of the

incident light and then travel back the high reflective media. This kind of wave

generated is defined as evanescent wave.

2.2.4 Condition for Surface Plasmon Resonance

Surface plasmon resonance occurs when the wave vector of the evanescent wave

matches the wave vector of the surface plasmons.

Though there are two original configurations in traditional SPR sensors, Otto

Configuration [4] and Krestschman configuration [5], the currently used SPR

biosensors are mainly based on Krestschman configuration. Therefore, to illustrate

the condition for surface plasmon resonance, Kretschmann configuration is used in

analysis. As shown in figure 2.4, it is composed of a prism and a sensor chip on it. The

sensor chip is a metal coated glass slide. When a p-polarized incident light passes a

prism through a metallic layer into a dielectric media, an evanescent wave will occur

at the interface of the two media.
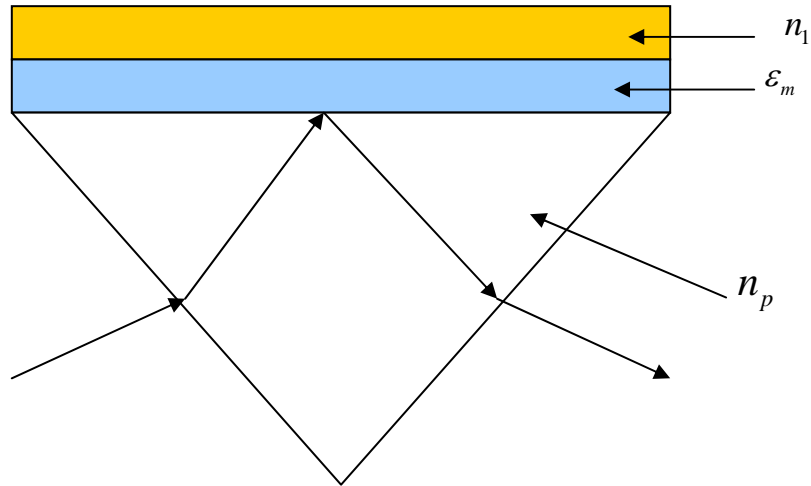
Figure 2.4 Kretschmann Configuration

The existence of the evanescent wave means that the energy of the incident light is absorbed and it will excite the surface plamons at the interface.

As introduced above, the wave vector of the evanescent wave is the component of the incident light's wave vector along the direction parallel to the surface of the metal layer, e.g.

$$k_{evan} = k_x \qquad \qquad (2.10).$$

When the angle of incident is α, k_x can be found as

$$k_x = \frac{\omega_0}{c} n_p \sin \alpha = k_{evan} \quad , \qquad (2.11)$$

where ω_0 is the frequency of incident light

n_p is the refractive index of the prism

α is the angle of incidence

c is the speed of light.

The wave vector of the surface plasmons k_{sp} is calculated by the following equation:

$$k_{sp} = \frac{\omega_0}{c} \sqrt{\frac{\varepsilon_m n_1^2}{\varepsilon_m + n_1^2}} \qquad (2.12)$$

ε_m = dielectric constant of metal layer

n_1 = refractive index of dielectric media

At a specific angle of incidence, the evanescent wave couples with the free electrons (SPs) on the surface of the metal layer, e.g.

$$k_{sp} = k_{evan} \qquad (2.13),$$

then the surface plasmon resonance will happen.

$$\frac{\omega_0}{c} \sqrt{\frac{\varepsilon_m n_1^2}{\varepsilon_m + n_1^2}} = \frac{\omega_0}{c} n_p \sin \alpha \qquad (2.14)$$

In this case, the incident angle α is regarded as the angle of surface plasmon resonance (SPR angle).

$$\alpha = \arcsin \sqrt{\frac{\varepsilon_m n_1^2}{(\varepsilon_m + n_1^2) n_p^2}} \qquad (2.15)$$

2.3 Working Principle of an SPR System

SPR instruments consist of three main units: the source of incident light, SPR sensing unit and detector [8] (Figure 2.5). There are three optical systems commonly used as the sensing unit to excite surface plasmons. They are systems equipped with prisms,

gratings and optical waveguides. Among them the prism equipped SPR system is mostly used in commercial SPR biosensors [8]. Krestschmann configuration is the most popular in commercial use because of its simplicity in the production. On the surface of currently commercially used SPR sensor chips, specialized component to capture the target component is immobilized, and it is called *ligand*. The target component is defined as *analyte*. All the components, such as ligand, buffer solution and sample solution, on the surface of the metal layer compose the sensing layer. As shown in Figure 2.4, the sensor chip is usually composed of a glass slide with metal coated on it surface. The materials of the metal layer ranges from Au to Ti and are introduced individually in part 2.6.2. The working temperature for SPR instruments are from 20 ^{o}C to 120 ^{o}C which means they can operate in normal temperature conditions and they are introduced in part 2.6.2 as well.
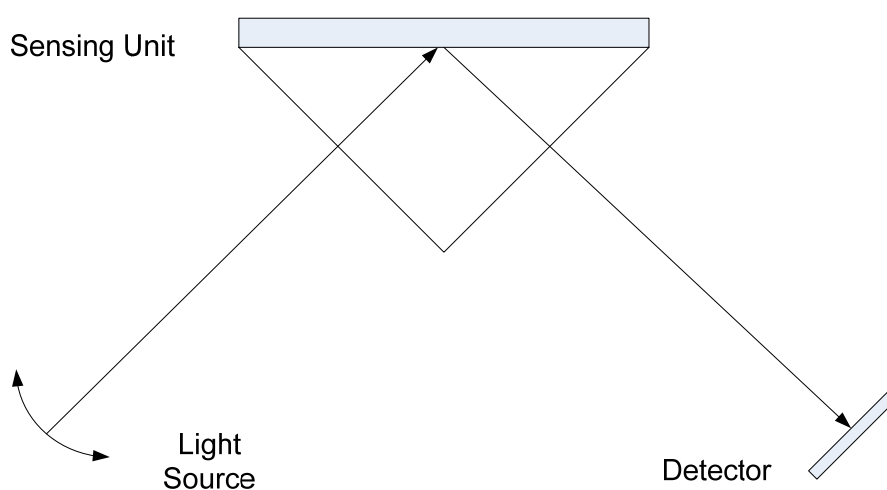
Figure 2.5 SPR instrument with light source, sensing unit and detector (arrows)

When the p-polarized incident light from the light source passes through the prism, the light will be reflected by the metal layer. The detector can measure the intensity of the reflected light when the incident angle is adjusted. At the angle that the minimum intensity of the reflected light happens, which is so called SPR angle, the maximum of surface plasmon resonance happens. SPR angle is based on the refractive indices on the sensing layer. When specific analyte is coated on the surface, which will be captured by the matching ligand on the surface of sensor chip, a change in refractive index happens. It will produce a SPR angle shift (A→B) as shown in figure 2.6, which is the evidence for the existence of such an analyte. The spectral width of an SPR curve, which usually refers to the FWHM (Full Width at Half Maximum) ranges from 2 to 8 degrees for commercial SPR sensors.
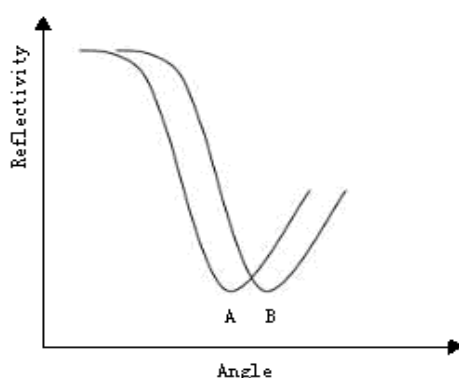
Figure 2.6 SPR curves (A) before and (B) after the binding of analyte (SPR angle)

Also, SPR biosensor can measure the wavelength shift when using incident light with

different wavelengths in the same incident angle. Same as the SPR curves which measures the change in the angle of incidence, at a certain wavelength (SPR wavelength), the minimum reflectivity will occur. The SPR wavelength will shift from A to B (Figure 2.7) in the same way as the SPR angle before and after the binding of analyte.
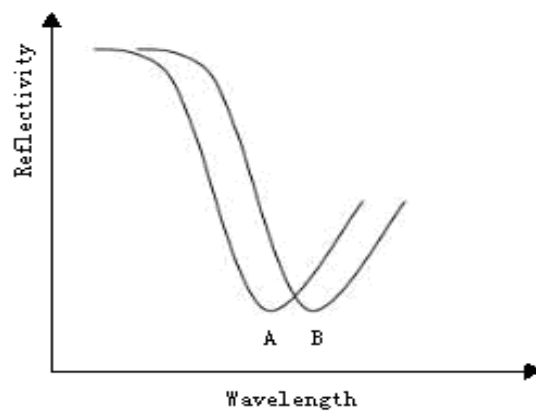
Figure 2.7 SPR curves (A) before and (B) after the binding of analyte (wavelength)

2.4 SPR Measurement

As a widely accepted bio-detecting technology, SPR has the advantages of label-free and real-time measurement. The complete process of an SPR measurement is presented. It starts with an injection of a buffer solution and ends by the removal of all buffer, ligand and analyte with a special regeneration solution.

2.4.1 Label-free Measurement

As discussed in part 2.3, the resonant angle changes with the change of the refractive index of the sensing layer. As shown in figure 2.6, the resonant angle shifts from A to B when the specific analyte is captured by ligand, otherwise, the angle shift will not happen. When a specific component needs to be detected among a large amount of unknown samples by SPR biosensor, there is no need to label every sample if a proper ligand is chosen. This label-free characteristic of SPR saves time and is an advantage over other biosensing techniques.

2.4.2 Real Time Measurement Curve

Another advantage of SPR technology is that it can measure changes in resonant angle and the reflectivity in real time, which enables it to get the real-time statistics of the volume of analyte bonded on the sensor chip and the bonding kinetics.
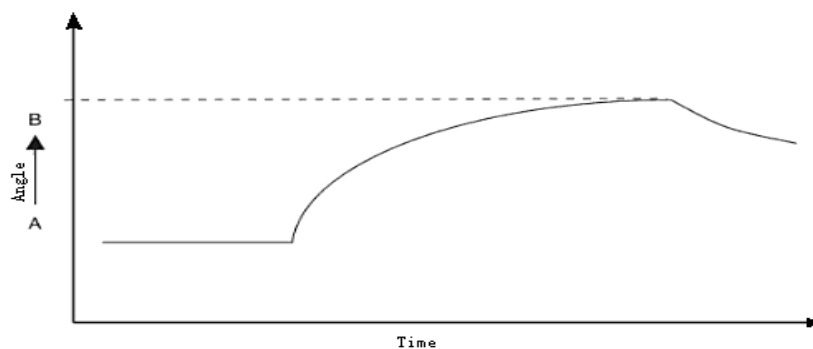
Figure 2.8 A Sensorgram: SPR angle vs. time

A sensorgram like Figure 2.8 shows the change of SPR angle vs. time. A indicates the

original SPR angle with only ligand in the buffer solution and B is the SPR angle after

the capture of the analyte.

A sensorgram can be expressed in SPR angle shift vs. time or reflectivity vs. time. It

can be compared with an SPR curve (Figure 2.9 and Figure 2.10). When a

sensorgram showing the SPR angle shift in real time is plotted, by rotating an SPR

curve, the two minimum reflection points with A and B correspond to the sensorgram

(Figure 2.9). The same application can be used to determine the reflectivity (reflected

intensity) shift at a specific angle on an SPR curve by comparing the reflectivity

change in the sensorgram (Figure 2.10).
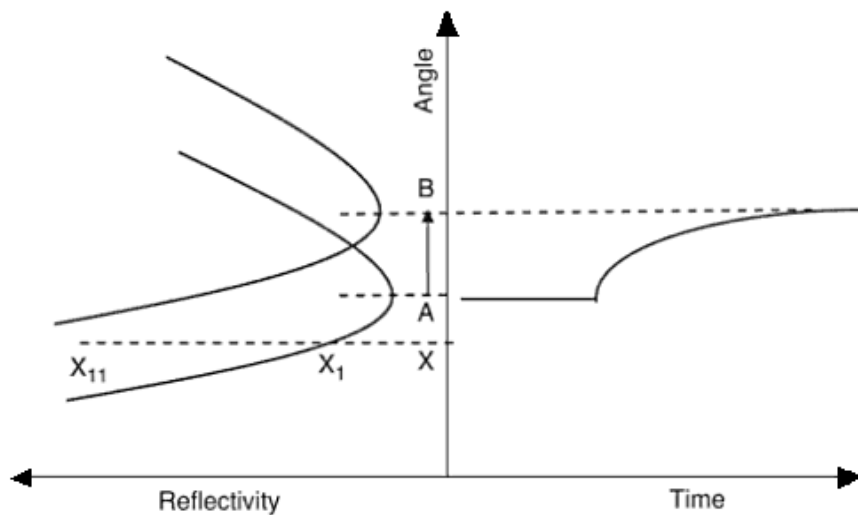
Figure 2.9 SPR angle vs. time, from a sensorgram to an SPR curve
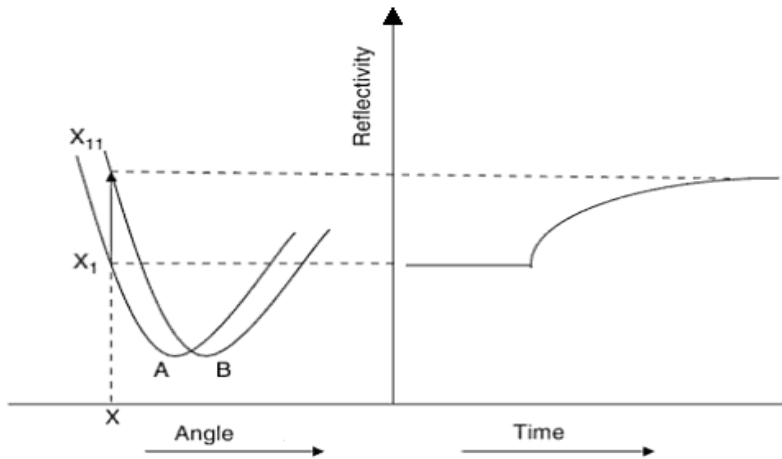
Figure 2.10 Reflectivity vs. time, from a sensorgram to an SPR curve

2.4.3 Process of SPR Measurement
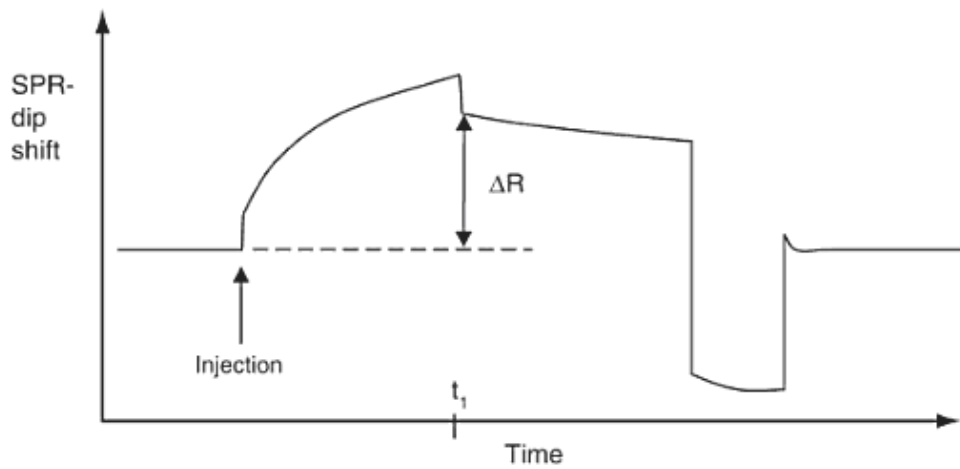
Figure 2.11 Full process of SPR measurement [8]

Figure 2.11 shows the full process of an SPR measurement. The process of a typical

SPR test starts with injecting a buffer solution to the surface of sensor chip. At the first

part on the sensorgram, the SPR angle reaches a stable situation after the injection of

the buffer solution. Then the sample solution is injected. A shift in the SPR angle will be produced if the analyte is captured. To make sure that the analyte is fully captured by the ligand, a continuous injection of the sample solution should be provided. However, during this step, some other components of the sample may be bonded on the surface of the sensor, which makes the test non-specific. Therefore, to eliminate these non-specific components, buffer solution should be injected to the sensor surface for a second time. The SPR angle drops immediately after the injection, thus, the proper amount of the captured target component can be obtained from ΔR. In addition, with the second injection of the buffer solution, the process moves to the dissociation step. The SPR angle begins to decrease according to the sensorgram because of the continuing injection of buffer solution. Regeneration solution should be injected on the surface of the sensor as the final step, in order to break the binding between analyte and ligand. To ensure that the sensor chip can be reused, it is important to make sure that enough regeneration solution is injected and the bonded analyte is cleared completely. The buffer solution will be injected again to start the next cycle of testing.

2.5 Application of SPR technology in Biosensing

The concept of biosensors is defined as *analytical devices comprised of biological element and a physicochemical transducer* [8]. Biosensors based on SPR techniques are first introduced to monitor the biomolecular interaction by Lundstrom in 1983 [7].

After that, SPR biosensors were brought into commercial use when Biosensor AB, the world leading commercial biomolecular sensing company, chose them as their platform in 1990 [37]. After the first commercial model of SPR biosensor was launched, other companies joined the manufacturer list of SPR biosensors and models with different functions were introduced.

SPR biosensors have become a well established method in biomolecular detection since its first commercial SPR biosensors [38]. Figure 2.12 shows both qualitative and quantitative biomolecular application of SPR biosensors. The application of SPR biosensors ranges from determining the concentration of molecules [39] to analyze the kinetic and affinity procedure in reaction [40].
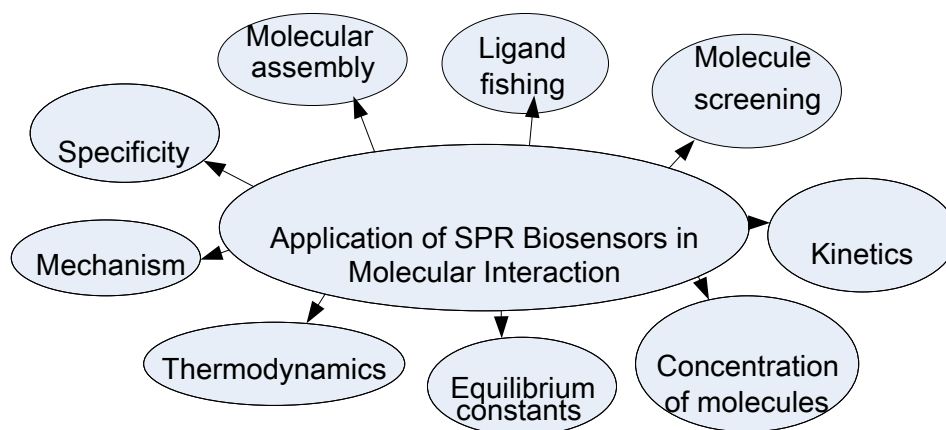
Figure 2.12 Biomolecluar applications of SPR biosensors

An example is introduced here to clearly demonstrate how the SPR technology is used in biomolecular interactions in terms of the interaction kinetics and concentration of molecules [41]. A SPR biosensor was used to analyze the concentration and the kinetics of gaseous hydrogen chloride (HCl). Polymers films on the surface of SPR biosensor were exposed to gaseous HCl which generates systematic modifications of SPR response curves [Figure 2.13 and Figure 2.14].
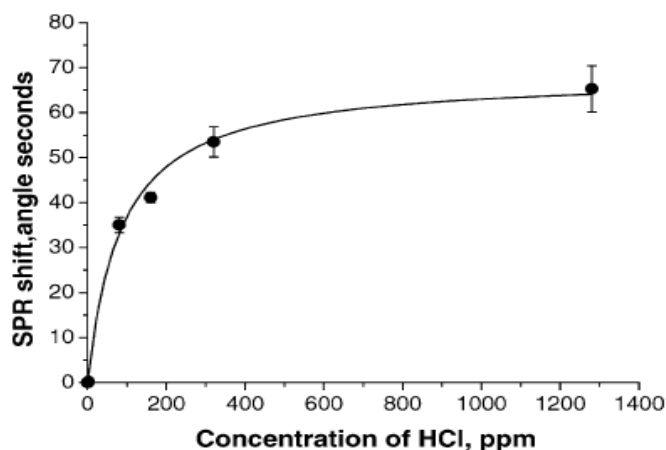
Figure 2.13 Dependence of SPR angle shift on the concentration of HCl
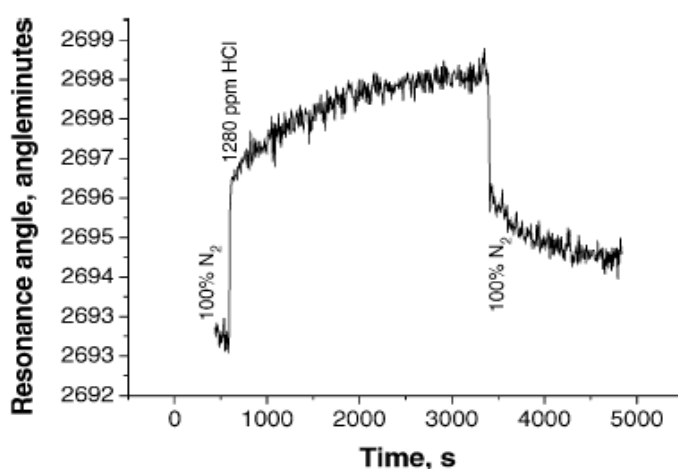
Figure 2.14 Kinetics of SPR angle shift on exposure to HCl

Figure 2.13 show that the SPR angle changes with the concentration of HCl changes.

In bio-sensing, comparing the testing results with figure 2.13, the concentration of HCl

can be confirmed. Figure 2.14 shows that the kinetics of SPR angle shift on the

exposure to HCl, i.e. the mass transportation of HCl. From this example, the way that

SPR technology is used for bio-sensing is more clearly explained.

With the ability to detect biomolecular interaction, SPR has been applied in different

areas in bioscience, ranging from drug development [42], biochemistry [43],

autoimmune diseases studies [44], clinical diagnostics [45] to food analysis [46].

Figure 2.15 shows examples of SPR applied in bioscience filed.
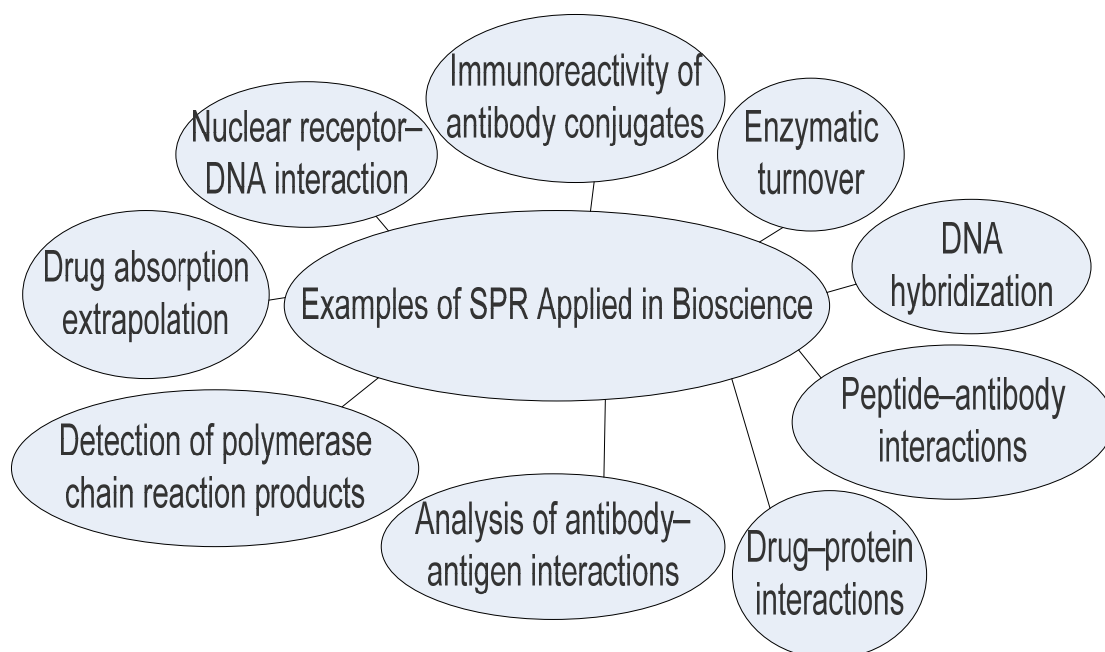
Figure 2.15 Examples of SPR applied in bioscience [47]

Since SPR biosensors have been widely used in various fields of biomolecular detection, along with BIACore, more and more corporations have launched different kinds of SPR products. Table 2.1 contains most of companies involved in the industry currently around the world.

Table 2.1 SPR biosensor manufacturers

SPR Biosensor manufacturers	Country	URL
Biacore Life Science	Sweden	www.biacore.com
Biosensing Instrument	USA	www.biosensingusa.com
Analytical –Systems	Germany	www.biosuplar.com
Reichert	USA	www.reichertai.com/
Moritex	UK	www.moritex.com
Potrel GBR	Germany	www.optrel.de
Toyobo	Japan	www.toyobo.co.jp
EcoChemie	Netherlands	www.ecochemie.nl
Sensia	Spain	www.sensia.es
NeoSensors	UK	www.neosensors.com
Nomadics	USA	www.nomadics.com
K-MAC	Korea	www.k-mac.co.kr
Lumera	USA	www.lumera.com

Table 2.1 (continue) SPR biosensor manufacturers

SPR Biosensor manufacturers	Country	URL
IBIA Technologies	Netherlands	www.ibis-spr.nl
Resonant Probes	Germany	www.resonant-probes.de
GenOptics	France	www.genoptics-spr.com
DKK-TOA	Japan	www.dkktoa.net
Nanofilm Surface Analysis	Germany	www.nanofilm.de
Bio-Rad	USA	www.bio-rad.com
GWC Technologies	USA	www.gwctechnologies.com
Plasmonic Biosensor	Germany	www.plasmonic.de
Graffinity Technologies	Germany	www.graffinity.com

The applications of SPR techniques in biosensing, along with the capability of detecting molecular interaction have proved that SPR is a useful and reliable method when applied in biosensors.

2.6 Current Research in Improving Sensitivity of SPR biosensors

Numerous research projects have been conducted to improve the sensitivity of SPR biosensors and they are briefly reviewed in this section. By discussing the current

research situation of the sensitivity of SPR biosensors, the main objectives of the author's project will be confirmed. Current research projects about the sensitivity of SPR biosensors were carried out in two aspects, the measurement of the sensitivity of SPR biosensors and the improvements of it. Measurements of it were based on several parameters regarding to the sharpness of the SPR curve, the resonant angle shift to the refractive index change in the sensing layer and the integrated sensitivity performance. Research to improve the sensitivity of SPR biosensors included new types of SPR sensor [22-30, 48], different coupling of SPR sensor [7, 49], and materials and thickness of the metal films on the SPR sensor chip [17-21].

2.6.1 Parameters of Sensitivity

Although current SPR biosensors are more sensitive than other label-free biosensors, they can hardly detect interactions between small molecular (few hundreds of Daltons) or molecules in low concentrations (physiological concentration) [12]. The sensitivity of SPR biosensors is defined as the derivative of recorded parameters such as reflectivity, resonant angle shift and wavelength, with regard to the controlled parameters (refractive index, incident angle, thickness of layer, etc) [50]. From SPR response curves (Figure 2.16), SPR sensor chips with higher sensitivity produce larger resonant angle shift and/or sharper SPR response curves, which can increase the detection limit and/or signal/noise ratio. Full width half maximum (FWHM), resolution and the intrinsic sensitivity are representative parameters to value the

sensitivity of SPR sensor chips and they are introduced accordingly.

SPR curve
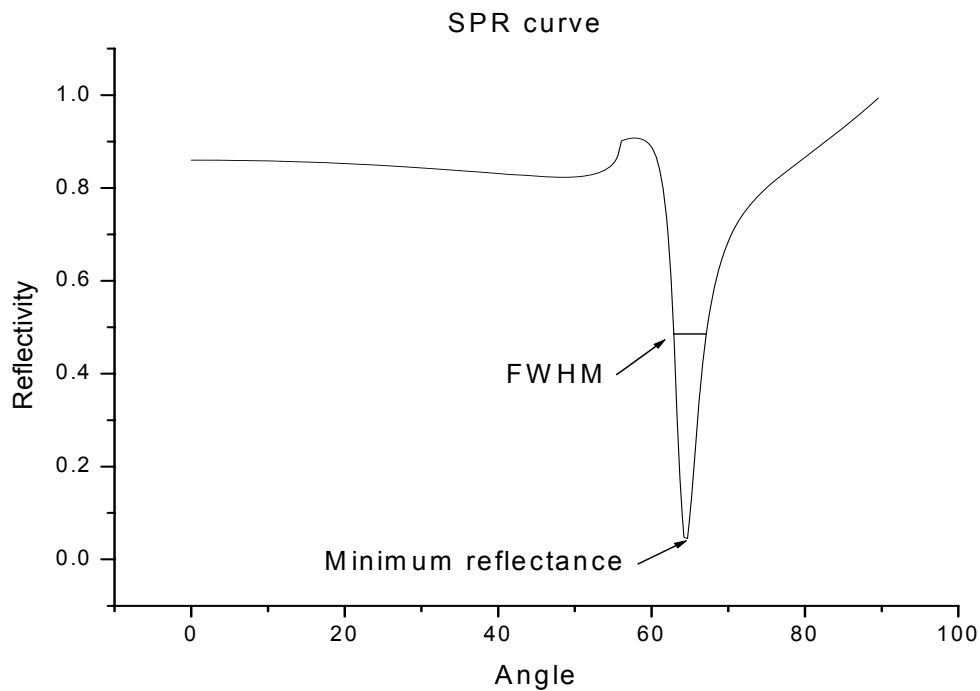
Figure 2.16 SPR response curve with minimum reflectance and FWHM

FWHM and minimum reflectance can be read from the SPR response curve as shown in Figure 2.16 and resolution and the intrinsic sensitivity are calculated from them.

◆ **FWHM (Full Width at Half Maximum)**

FWHM is defined as an expression of the extent of a function, given by the difference between the two extreme values of the independent variable at which the dependent variable is equal to half of its maximum value [51]. On an SPR curve, FWHM is the width of the curve, in degrees, at which the reflectance is the half of the maximum, as

show in Figure 2.17. As defined, FWHM represents the width of a reflection curve. The narrower the SPR curve is, the higher signal/noise ratio the SPR sensor chip holds, thus the easier it is to determine the SPR angle from the SPR curve.
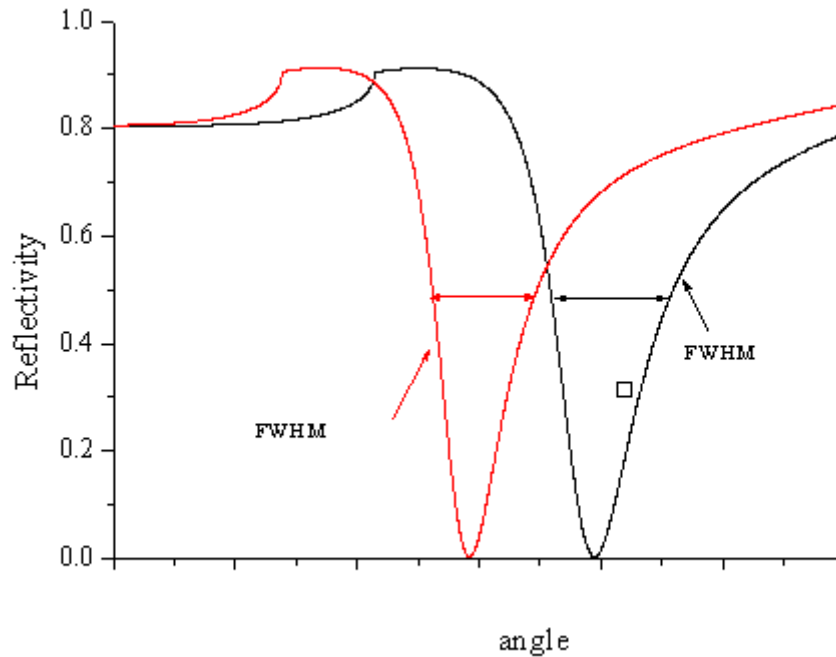
Figure 2.17 FWHMs in SPR curves

◆ **Resolution**

The term resolution is proportional to the difference between the maximum and minimum reflectance, and inversely proportional to FWHM. It is functioned as follows:

$$\text{Resolution} = \frac{R_{max} - R_{min}}{FWHM} \qquad (2.16)$$

The minimum reflectance is the reflectance when the maximum of surface plasmon resonance happens as shown in figure 2.16, and the maximum reflectance can be read from figure 2.16 as well.

Based on Eq.2.16, it can be observed that high resolution means either a small FWHM or a large difference between the maximum and minimum reflectance, which represents a sharp SPR curve and a high signal/noise ratio of the SPR sensor chip,. A sharp SPR curve can minimize the error in determining the exact value of the resonant angle. Sensor chips with higher resolution are able to detect smaller changes in the parameters of the SPR sensing device which are usually limited by the noise of SPR instruments [50].

◆ **Intrinsic sensitivity**

When an analyte is captured, the SPR resonant angle will shift due to the change of the refractive index of the sensing layer. For the same change of the refractive index of the sensing layer, an SPR sensor chip with good sensitivity produces larger SPR angle shift so that it can be easily discovered. The resonant angle shift and FWHM are two general aspects to determine the performance of an SPR biosensor. To take both of them into account, intrinsic sensitivity (IS) [52] is calculated by dividing resonant angle shift with the product of FWHM and the refractive index change in the sensing layer.

$$IS = \frac{\Delta\theta}{FWHM \times \Delta n} \quad (2.17),$$

where $\Delta\theta$ is the resonant angle shift corresponding to the refractive index change in the sensing layer and Δn is the refractive index change in the sensing layer.

From the definition, for the same refractive index change of the sensing layer, high IS means either a large shift in the resonant angle or a smaller FWHM. Both of them represent better sensitivity performance of SPR biosensor. Therefore, IS is an important sensitivity parameter which represents the integrated sensitivity performance of SPR biosensor.

2.6.2 Current Research to Improve the Sensitivity of SPR Biosensor

The current research to improve the sensitivity of SPR biosensors includes different coupling modes, operational wavelength, nano-structures on the surface of sensor chip, different materials of metal films, and the thickness control of the metal films.

✓ **Coupling modes of SPR biosensors**

A sensitivity comparison of different coupling modes of SPR biosensor was studied by F.C.Chien [12] in 2004. They were the conventional SPR, the long range SPR (LRSPR), the coupled-plasmon waveguide SPR (CPWR) and the waveguide coupled SPR (WCSPR) (Figure 2.18). The sensitivities of these four SPR modes with different couplings were studied in angular detection.
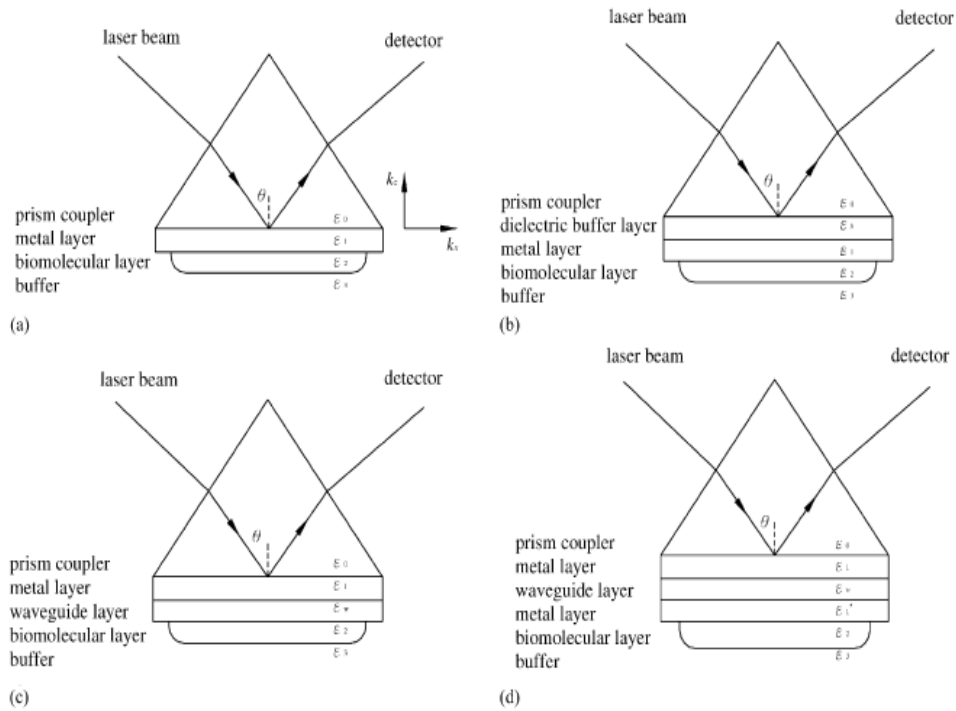
Figure 2.18 Coupling modes of SPR biosensors: a) conventional SPR; b) LRSPR; c) CPWR; and d) WCSPR [12]

SPR curves of the four coupling modes are shown in figure 2.19, and the resonant angle shifts of them are shown in table 2.2, conclusions were drawn that although LRSPR and CPWR presented narrower SPR curves than conventional SPR, their angular detecting range were restricted in resonant angle around 50 degrees so that limits their detection [12]. The conventional SPR produced the largest angle shift in the same condition but a slightly wider SPR curve. The WCSPR produced angle shift only slightly smaller than that of the conventional SPR and a narrower SPR curve. Considering two important aspects of sensitivity performance of SPR biosensors, the narrowness of SPR curve (FWHM) and the resonant angle shift, the conventional SPR and WCSPR are better choices than the other two coupling modes. Those

results provided valuable information of the different coupling modes of SPR

biosensors, thus enabled researchers to choose the proper SPR biosensor in specific

research.
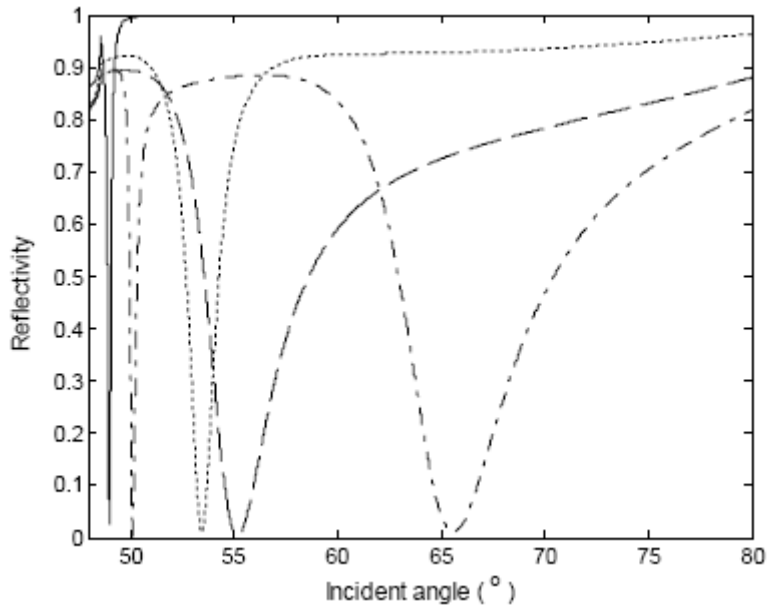
Figure 2.19 SPR curves for the four modes (solid line: LRSPR, dashed line:

conventional SPR, dotted line: WCSPR, dashed-dotted line: CPWR) [12]

Table 2.2 Resonant angle shifts for the four modes in degrees

Conventional SPR	LRSRP	CPWR	WCSPR
0.2714	0.0293	0.0329	0.1523

✓ **Operation wavelength on the sensitivity of SPR biosensor**

The effect of the wavelength of the incident light on the sensitivity of SPR sensors was

studied by several researchers in the 21st Century by Nitikin and Valeiko, etc. [13, 14].

The sensitivity of SPR biosensor in aspect of the angle shift according to the refractive

index change of the sensing layer was found by J. Homola to increase by the

decreasing of the wavelength [15]. In comparison, by the same person [16], the

sensitivity of SPR biosensor in aspect of the resonant wavelength shift corresponding

to the refractive index change of the sensing layer was discovered to increase when

the incident wavelength increases. Although in the latter situation, higher wavelength

produces sharper reflectance curves [8]. However, the increase in wavelength was

found to result in the increase in the penetration depth of the evanescent wave at the

interface. This allows the sensor to be more sensitive to the dielectric change far from

the interface which makes the sensitivity of SPR equipments inaccurate. A reasonable

range for wavelength of the incident light is from 600 nm to 750 nm [8].

✓ **LSPR and nano-patterns**

Regarding to the SPR sensor chip, research has been carried out in order to find new

type of sensor chips along with the conventional SPR sensor chips or make

improvements depending on the conventional SPR sensor chip. As a new type of

SPR sensor chip, localized SPR (LSPR) sensor chips were introduced by using metal

particles or rough structures as the surface of the sensor chips [22-29]. LSPR was

found to increase the signal/noise ratio when used on small scale sensor chip by the

localization of electro-magnetic field.   However, it was concluded by A. J. Haes in

2002 [30] that the detection capability of LSPR sensor chip is far poorer than conventional SPR sensor chip when used on large SPR instruments. Although nanostructures on the surface of LSPR sensor chip were developed quickly in recent years, it was still struggling in the application of large scale SPR instruments [30].

✓ **Materials of the metal films**

As SPR happens at the interface of metal and dielectric material, several metals, for example, Al, Co, Cu, Au, Fe, Pb, Ni, Pd, Pt, Ag, Ti, were used as the metal film on the surface of SPR sensor chip [53] to study the effect of dielectric constants of the metal layers on the sensitivity of SPR sensor chips. Results showed that the narrowness of the SPR reflectance curve is mainly dependent on the metal's dielectric constant. Among all the metals that have been used, gold and silver are most widely used metals on the SPR sensors. Gold produces large SPR resonant angle shift while its response curve is relatively wider than that of silver. As the real part of silver's dielectric constant is slightly larger than that of gold's, it produces narrower SPR curves than gold. The theoretical results of the narrowness that silver provides led to some attempts in using it as the coating on the surface of SPR sensor chip [17-20]. However, all the attempts showed that silver is chemically unstable and is easily oxidized. It needs a dielectric protection layer on it which has a negative impact on the sensitivity of SPR sensor chip [17, 18]. Although gold produces wider SPR curve than silver, it is more popular being the surface of SPR sensor chips with its stable

chemical property.

✓ **Thickness of the metal films**

Research was also carried out to study the effect of thickness of the metal layers on the sensitivity of SPR sensor chips at different operation temperature by B.A. Snopok in 2001 [21]. The research was conducted by analyzing the SPR curves of different thickness of gold layer and temperature, the result is shown in figure 2.20. In order to generate better sensitivity, narrower SPR curves need to be generated. Results showed that $R_{\min}$ can be made very close to zero when metal layer with appropriate thickness is deposited. From the results, a gold film with thickness of 45nm performed the best sensitivity. The optimal thickness of gold film ranges from 40nm to 50nm. Furthermore, the SPR sensor chip provided a better sensitivity when operated in high temperature at 120 degree than in 20 degree. However, the difference of the SPR curve between these two operational temperatures was not so high that SPR biosensor can operate in normal temperature.
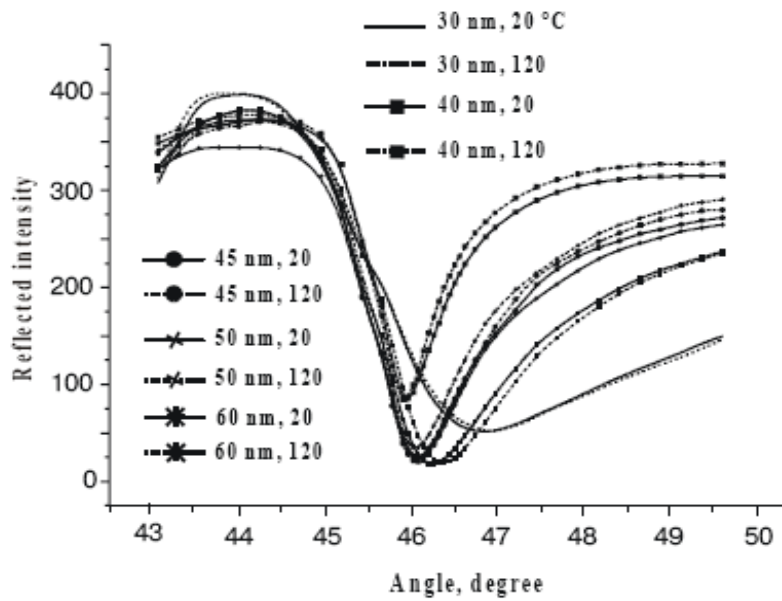
Figure 2.20 SPR curves regarding to different thickness of metal layer and operational temperature [21]

2.6.3 Proposed Objectives to Improve the Sensitivity of SPR Sensor Chips

Two new methods to improve the sensitivity of SPR sensor chips, the silver/gold bimetallic layer sensor chip and the roughness effect of the sensor chip surface, are raised as the main objectives of the project after reviewing the existing methods.

As the project is aimed on the improvement of sensitivity of SPR sensor chip, which regards to the conventional SPR sensor chip, methods based on LSPR and nanostructures are not suitable although they are developing fast. Furthermore, the project is mainly focused on the sensor chip but not the other aspects of SPR instrument, such as wavelength or waveguide coupling.

◆ Bimetallic layer sensor chip

As mentioned above, silver and gold perform differently in surface plasmon resonance and have their unique advantages as well as disadvantages. One way to take the advantages of both materials is to construct bimetallic SPR sensor chips coated with silver as the inner layer and gold as the outer layer. This method takes the advantage of outstanding performance of signal/noise ratio of silver and good detection limit of gold, at the same time, it protects the silver layer from oxidization by the outer gold layer. By using this method, SPR sensor chip is predicted to hold both a narrow SPR curve and a large response to the changes in the refractive index, which improve its sensitivity in both signal/noise ratio and detection limit.

◆ Roughness analysis of SPR sensor chip

Apart from the bimetallic layer SPR sensor chip, the analysis of the surface roughness of SPR sensor chip is another main objective of the project. The SPR sensor is conducted basically with a glass slide and a thin metal film on the surface on it. In the current research of SPR sensor chip and methods to improve the sensitivity of SPR sensor chip, it is assumed that the surface of the sensor chip is planar, which is not true in reality. The ignorance of the realistic surface roughness of the sensors causes compromise of the sensor sensitivity. Roughness of metal film on glass slides has been analyzed by depositing an intermediate layer (such as MgF_2, CaF_2, LiF) onto

glass slides by G. J. Kovacs and E. Fontana [54, 55]. It's reported that the sensitivity of SPR sensor chip can be improved by optimizing the surface roughness of the gold layer. However, considering that the metal film is coated on the surface of glass slide thus the roughness of it is dependent on the roughness of the glass slide. Therefore, the roughness effect of glass slide is predicted to influence the sensitivity of SPR sensor chip as well. The roughness effect of glass slides was investigated by both computational and experimental methods by the author. Parameters of sensitivity generated by different glass slide roughness condition were studied and results showed that the roughness of glass slide do affect the sensitivity of SPR sensor chip.

2.7 Conclusions

SPR biosensing technology has been applied into lots of aspects ranging from biomedical detecting to biochemical sensing since the appearance of the first biosensor based on it. The biomedical and biochemical applications of SPR techniques are more than likely to widen in the future with the improvements of the technology.

SPR sensor chip, as an important part in a SPR biosensor, plays a vital role in improving the sensitivity. To evaluate the sensitivity of SPR sensors, the most important parameters are FWHM, minimum reflectance, resolution and resonant angle shift. SPR sensor chips that produce sharp SPR curves and large angle shifts

represent a better sensitivity. In addition, research has been carried out to study the effects of the thickness and dielectric constants of the metal layers, the wavelength of the incident light, different coupling modes and new types of SPR biosensors on the sensitivity of SPR biosensors.

After the complete literature review, conducting the silver/gold bimetallic sensor chip to enhance the sensitivity of SPR sensor chip and studying the roughness effect of the sensor chip on its sensitivity were decided to be the objectives for the project.

3. BIMETALLIC LAYER STRUCTURES FOR SPR SENSORS

3.1 Introduction

This chapter presents a study on the structure of gold/silver layer SPR sensor chips. There is a growing interest in improving the sensitivity of SPR biosensors since SPR was first introduced in 1982 for gas detection [6]. Attempts such as polarization of the incident light [13-16], a waveguide propagation of light [12] and using nanoparticles on the sensor chip surface [22-29] have been made to improve the sensitivity. The work presented in this chapter is focused on bimetallic layer sensor chips. Silver and gold perform differently in Plasmon resonance when they are used as coating materials on glass slides. Silver produces a narrower SPR curve, indicating a higher signal/noise ratio. But it is chemically unstable and tends to be oxidized relatively quickly. Gold is more chemically stable and its Plasmon resonance curve possesses a high resonant angle shift corresponding to the changes of refractive index in the sensing layer. One way to take the advantages of the both metals is to construct the SPR sensors with a silver layer at the bottom and a thin gold layer on the top to reduce oxidation. The bimetallic sensor chips were simulated and designed based on Fresnel's equations. The refractive index of the sensing layer was changed by using different buffer solutions.

3.2 Simulation

Computer simulation has been extensively used in the bimetallic layer SPR sensor design and comparison with monolayer SPR sensors in this project. Winspall was used throughout the simulation. Winspall is a software package for simulation of surface plasmon resonance performance based on the Fresnel equations [56]. The thickness, refractive index can be entered, the dielectric constant is calculated according to the Fresnel's equation [57] and the SPR curve is plotted. A typical response curve by Winspall is shown in figure 3.1, from which, the minimum reflectance, FWHM, resonant angle can be analyzed. However, the assumption that the surface of the SPR sensor chip is planar results in that the roughness of every layer on the surface of the SPR sensor chip is ignored in the software package. Therefore, in the simulation of the bimetallic layer system, all the layers on the surfaces of the SPR sensor chips are assumed to be planar.
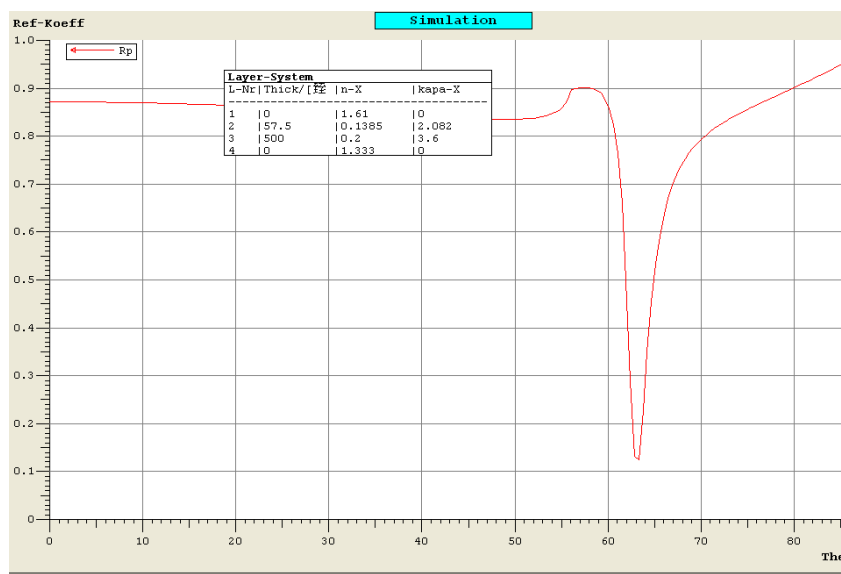
Figure 3.1 SPR response curve by Winspall

As discussed previously in 2.6.2, the most suitable thickness of metal layer to be deposited on the sensor chip surface ranges from 40 nm to 50 nm. Simulations were carried out by assuming that the total thickness of metal layers on the surface of SPR sensor chip is 50 nm. Silver/gold films with different thickness combinations were studied. Water and ethanol were used to change the refractive index of the sensing layer.

Table 3.1 Parameters used in simulation

Layer	Refractive index		Layer thickness
	n	k	
Glass	1.61	0	
Silver	0.135	3.988	50nm to 0nm
Gold	0.2	3.6	0nm to 50nm

The refractive index and thickness of layer used in simulation is listed in table 3.1. For the sensing layer, the refractive index of water is 1.333 and that of ethanol is 1.36. Minimum reflectance, FWHM and resolutions were obtained by using water as the buffer solution. SPR angle shift were achieved when water and ethanol were used consecutively, as they had different refractive index.

3.3 Results and Discussion

The sensitivity parameters for silver/gold sensor chips with different thickness combinations were compared. The simulation results of these parameters are discussed as follows.

◆ **FWHM**

The relationship between FWHM and the combinations of silver and gold is shown in figure 3.2. X axis is the combination of bimetallic sensor chips with the decrease in the thickness of silver layer. Y axis represents the FWHM in degrees. FWHM is observed to increase with the decreasing in the thickness of silver layer and at the same time the increasing in the thickness of the gold layer. This indicates that silver produces much narrower SPR response curves compared with gold.
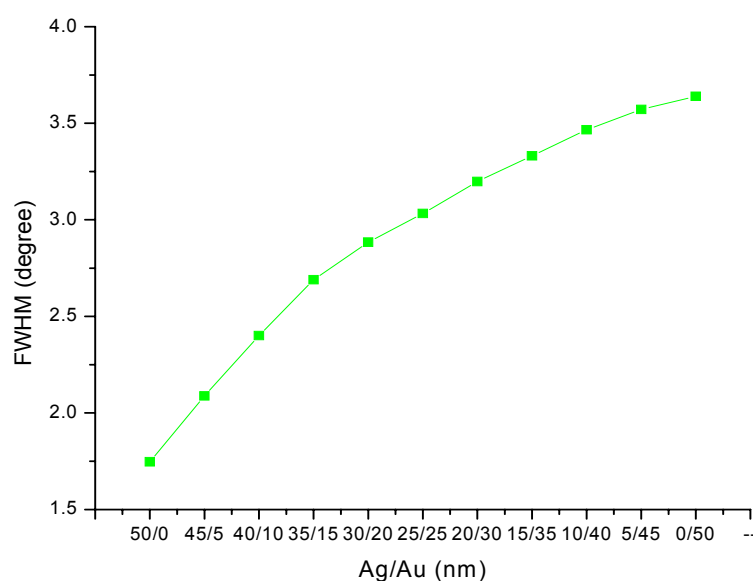
Figure 3.2 FWHMs of different Ag/Au combinations

◆ **Resolution**

As shown in figure 3.3, the mono-silver layer sensor chip possesses the highest resolution when the mono-gold layer one produces the lowest resolution. The resolution of the bimetallic sensor chips drops when the thickness of silver decreases. After the combination of silver and gold with 35nm of sliver and 15nm of gold, the bimetallic sensor chips produce nearly the same resolution as the monolayer sensor chip with gold only.
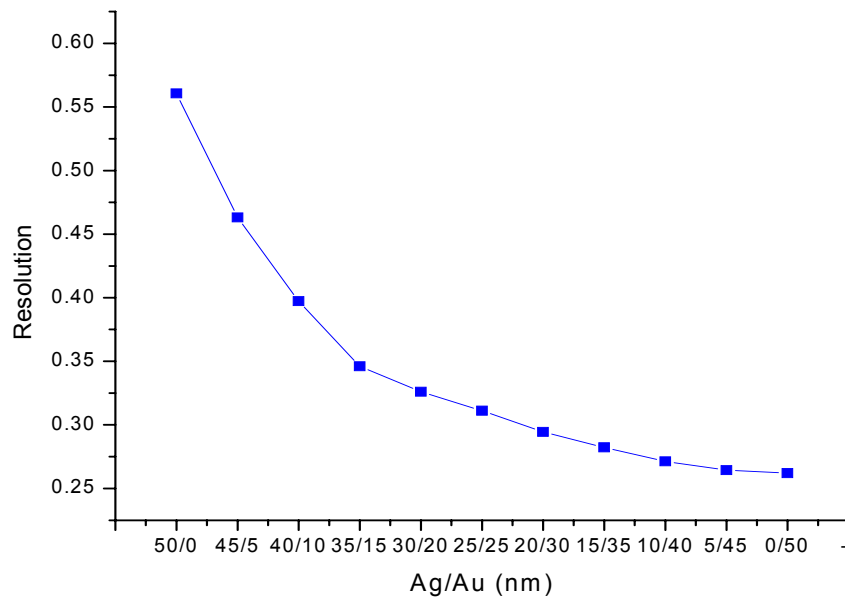
Figure 3.3 Resolutions of different Ag/Au combinations

◆ **Intrinsic sensitivity**

Figure 3.4 shows the intrinsic sensitivity corresponding to different thickness combination of silver and gold. Regarding both aspects of the resonant angle shift according to the change in refractive index and FWHM, IS decreases with the decrease of the thickness of silver in the bimetallic layer system, which indicates that

the integrated sensitivity of the SPR sensor chip drops while the thickness of silver decreases and that of gold increases. The mono silver layer sensor chip produces the best intrinsic sensitivity.
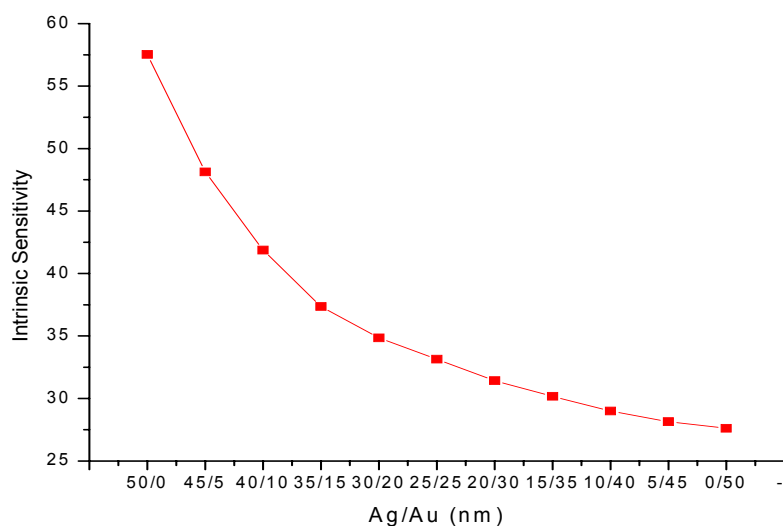
Figure 3.4 Intrinsic Sensitivity of different Ag/Au combinations

It was found that bimetallic sensor chips with silver layer thinner than 40nm and gold layer thicker than 10nm produced similar resolution and FWHM as the mono gold layer sensor chip. The best choice of thickness combination among all the bimetallic sensor chips is 45nm thick silver and 5nm thick gold. It produced narrower SPR response curve than the mono gold layer sensor chip and possess higher intrinsic sensitivity while considering both the narrowness of SPR curve and the resonant angle shift due to the change of refractive index in the sensing layer. It produces high sensitivity performance similar to the mono silver layer and with protective gold layer at the same time.

3.4 Conclusions

SPR sensor chips coated with silver produce narrower and sharper SPR response curves, due to the real part of its dielectric constant is slightly higher than that of gold, but it has the disadvantage of poor chemical stability. A computer simulation study on the silver/gold bimetallic sensors has resulted in an optimal combination of 45nm thick silver and 5nm thick gold layers. The SPR sensors with these silver/gold layers produce narrower SPR response curves and better integrated sensitivity performance than the sensors with a mono gold layer, more similar to a mono silver layer sensor chip. At the same time, the gold layer at the surface protects silver from being oxidized. The optimal silver/gold bimetallic sensor design perform better than the currently used mono gold layer SPR sensors and has the potential to be widely adopted in SPR biosensors.

4. THEORETICAL ANALYSIS OF SURFACE ROUGHNESS EFFECT ON SENSITIVITY

4.1 Introduction

The theoretical analysis of surface roughness effect of glass slide on the sensitivity of SPR sensor chip is presented in this chapter. In the current studies of SPR sensor chips, as well as the bimetallic layer sensor chips introduced in chapter 3, the surfaces of the sensor chips are assumed to be perfectly smooth. However, the angular dependence and polarization of light have been proved to be affected by the surface roughness as it causes light emissions in surface plasmons [58, 59]. Work has been carried out to investigate the influence of surface roughness of the metal layer on the sensitivity of SPR biosensors as mentioned in the literature review [54, 60]. What is less well known is the roughness effect of glass slides on the sensitivity of SPR sensor chips. This section describes a study on the surface roughness effect of the glass slide on the sensitivity of SPR sensors in theory and supported by simulation. A pseudo-layer between the metallic layer and dielectric layer is introduced to function as the rough surface in the simulation. The theoretical analysis shows that the sensitivity of SPR sensor chip can be improved by controlling the surface roughness of glass slide.

4.2 Theoretical Modeling

The pseudo-layer (Figure 4.1) is placed between the metallic layer and dielectric layer with an effective dielectric function calculated with Maxwell-Garnett Theory [54, 60]. It is introduced to replace the roughness area between the metal layer and dielectric layer. The pseudo-layer makes it possible to simulate the roughness effect of the glass slide in Winspall package since it solves the limitation of the software package that roughness of all the layers are included.
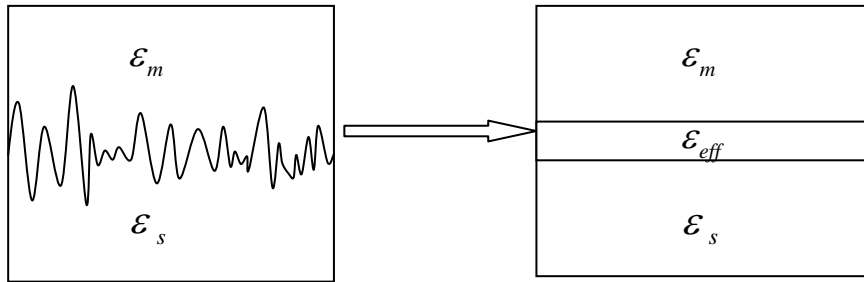
Figure 4.1 Pseudo-layer at the interface of layers

The effective dielectric function of the pseudo-layer can be calculated by the equation based on the Maxwell-Garnett theory [55],

$$\varepsilon_{eff}(\omega) = \varepsilon_m(\omega) \frac{[(3-2q)\varepsilon_s + 2q\varepsilon_m(\omega)]}{[q\varepsilon_s + (3-q)\varepsilon_m(\omega)]} \quad (4.1),$$

where ε_m is the dielectric function of metal layer,

ε_s is the dielectric function of the other layer (buffer or glass slide), and q is the volume fraction of the metal in the pseudo-layer.

The optical constants of all the materials can be obtained from the equation

$$\varepsilon = (n + ik)^2 \quad (4.2),$$

where ε represents the dielectric function of the material,

n is the real part of the refractive index of the material and k the imaginary part of it.

The modeling was based on mono gold layer SPR sensor chips. Water and ethanol were used as the buffer solutions to change the refractive index of the sensing layer. When the roughness effect of the glass slide was discussed, based on the fact that gold was deposited on the surface of a glass slide, there were two roughness areas: one at the interface between glass slide and gold layer, and the other at the interface between gold layer and buffer solution. Therefore, two pseudo-layers were introduced to replace them. (Figure 4.2)

| Buffer Layer |
| Pseudo-layer |
| Gold Layer |
| Pseudo-layer |
| Glass slide |

Figure 4.2 Pseudo-layers in the modeling

The effective dielectric constant of the pseudo-layer between the gold layer and the buffer solution was calculated by using the dielectric constant of buffer solution as ε_s and that of gold as ε_m in Eq.3.1. The effective dielectric constant of the one between glass slide and gold layer was calculated by Eq.3.1 using the dielectric constant of glass slide as ε_s and that of gold as ε_m.

4.3 Simulation

Simulation of roughness effect of the glass slide was conducted by using Winspall, as introduced in chapter 3. Thicknesses and refractive indices of different layers were required for simulation.

To obtain the refractive index of the pseudo-layers, volume fraction of gold particles in them and the thickness of them need to be determined and used in Eq 3.1. M Kanso [60] measured the roughness of gold film in his research in 2007, and found that reasonable volume fraction of gold in pseudo-layers can be chosen as q=0.5. Therefore, the volume fraction of glass in the pseudo-layer at the interface of glass slide and gold layer is p=0.5. The refractive indices of these two pseudo-layers were calculated with the volume fractions of gold, by using Eq. 3.1 and 3.2. Refractive indices used in the simulation of the roughness effect of glass slide are listed in table 4.1 and 4.2.

Table 4.1 Refractive indices of all the layers for the roughness effect of glass slide

(water as buffer solution)

Layer	Refractive index	
	n	K
Glass	1.61	0
Pseudo-layer	0.1531	1.8555
Gold	0.2	3.6
Pseudo-layer	0.1398	2.0164
Water	1.333	0

Table 4.2 Refractive indices of all the layers for the roughness effect of glass slide

(ethanol as buffer solution)

Layer	Refractive index	
	n	k
Glass	1.61	0
Pseudo-layer	0.1531	1.8555
Gold	0.2	3.6
Pseudo-layer	0.1408	2.0027
Ethanol	1.36	0

The thickness of the pseudo-layer can be obtained from a Gaussian function and calculated by $d = 2\sqrt{2}RMS$ (4.3). RMS is the root mean square roughness. From AFM measurement results of randomly chosen glass slides, RMS ranges from 0 nm to 2 nm. Therefore, for the simulation of the roughness effect of the glass slide, the thickness of the pseudo-layer at the interface of glass slide and gold slide is chosen to range from 1nm to 6nm so that the results are realistic. AFM results before and after the deposition of a gold layer showed that the RMSs on the surface of a gold layer are usually half of the RMSs on the surface of glass slide [55]. The thickness of the pseudo-layer at the interface of gold and buffer solutions was chosen to be half of that of the pseudo-layer at the interface between the glass slide and the gold layer in simulation. As the thickness of the pseudo-layer was contributed by that of the gold layer and the dielectric layer according to their volume fractions, the thickness values contributed to the pseudo-layer were excluded from them. The thickness values of gold layer and two pseudo-layers are listed in table 4.3.

Table 4.3 The dependence of gold layer thickness on thickness (nm) of pseudo-layers and volume fraction.

Pseudo-layer between glass and gold	Gold	Pseudo-layer between gold and buffer
1	49.25	0.5
2	48.5	1
3	47.75	1.5
4	47	2
5	46.25	2.5
6	45.5	3

The sensitivity of sensor chips with different roughness values was compared by measuring the FWHM, resolution and intrinsic sensitivity for different volume fractions and thickness of pseudo-layers.

4.4 Results and Discussion

The sensitivity parameters of the sensors with a certain degree of roughness, including the minimum reflectance, FWHM, resolution and resonant angle shift, are analyzed here.

◆ **FWHM**

As shown in figure 4.3, FWHM is observed to increase with the increase of the depth of the pseudo-layer. This implies that the SPR response curve becomes wider with the increase of the depth of pseudo-layer, which will increase the error to determine the resonant angle or angle shift.
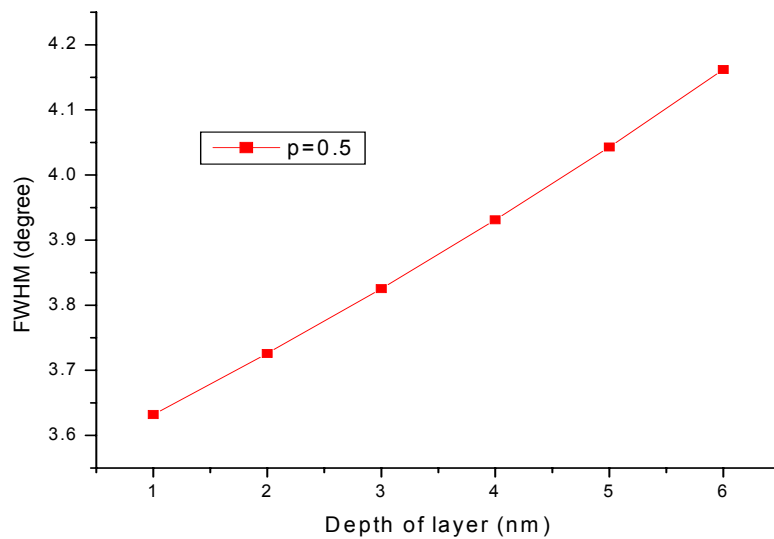
Figure 4.3 FWHM vs. depth of pseudo-layer (d)

◆ **Resolution**

From figure 4.4, the resolution decreases with the increase of depth of pseudo-layer, i.e. signal/noise ratio obtained from SPR curve becomes low with the increase of depth of the pseudo-layer, thus making the performance of the SPR biosensor worse.
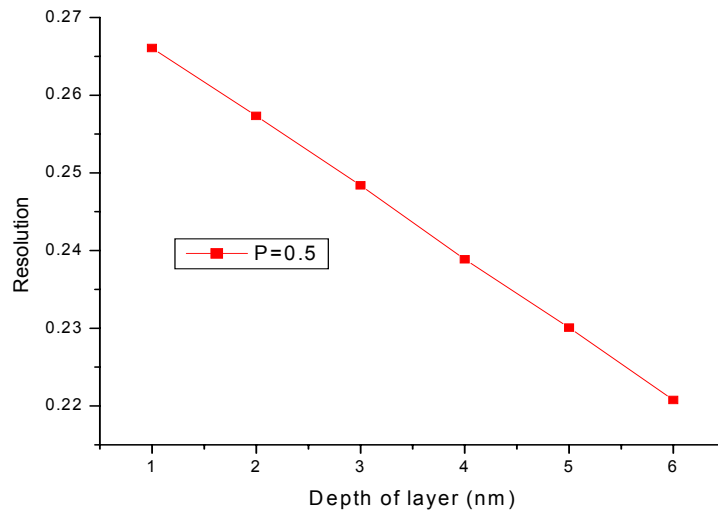
Figure 4.4 Resolution vs. depth of pseudo-layer (d)

◆ **Intrinsic sensitivity (IS)**

Figure 4.5 shows the intrinsic sensitivity corresponding to the depth of pseudo-layer.

As it takes both the change in refractive index and FWHM in to account, IS decreases

with the increase of the depth of pseudo-layer, which indicates that the integrated

sensitivity of the SPR sensor chip drops with the increasing depth of pseudo-layer.
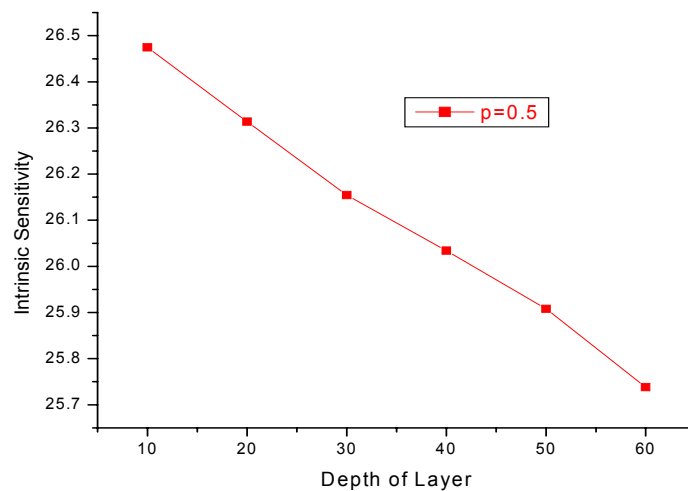
Figure 4.5 IS vs. depth of pseudo-layer

By analyzing the FWHM and the resolution, the SPR curve becomes wide with the increase of the depth of the pseudo-layer, which can increase the error in determining the resonant angle. The signal/noise ratio decreases with the increase of the depth of the pseudo-layer. All of these trends show clearly that the sensitivity of the SPR sensor chip gets worse with the increase of the depth of the pseudo-layer. The depth of the pseudo-layer is connected with the root-mean-square roughness of the glass slide (Eq 4.3), so that the sensitivity performance of the SPR sensor chip becomes poorer with rougher surface of glass slide in terms of the sharpness of the SPR curve.

IS decreases with the increasing depth of the pseudo-layer, which means the integrated sensitivity performance of both aspects of the sharpness of the SPR curve and the response to the refractive index change in the sensing layer becomes worse with rougher surface of glass slide.

4.5 Conclusions

The roughness effects of the glass slide on the sensitivity of SPR sensor chips are analyzed theoretically. The simulation results show that FWHM increases with the increase of the depth of pseudo-layer, while resolution decreases with it. Narrow and sharp SPR curves can be produced by making a smooth surface of the glass slide, which can minimize the error in determining the SPR resonant angle. Taking both the narrowness of SPR curve and the resonant angle shift into account, IS decreases with

the depth of pseudo-layer, which is closely related to the surface roughness of glass

slide. It can be concluded that the sensitivity performance of SPR sensor chip can be

improved by improving the surface roughness condition of the glass slides.

5. EXPERIMENTAL ANALYSIS OF SURFACE ROUGHNESS EFFECT ON SENSITIVITY

5.1 Introduction

This chapter presents the experimental analysis carried out to investigate the surface roughness effect of a glass slide on the sensitivity of SPR biosensor. It follows the simulation work described in chapter 4 to analyze the effect of surface roughness of glass slide on the sensitivity of sensor chips. In the experiments, sensor chips were fabricated to increase their sensitivity based on previous theoretical analysis.

The experimental work includes glass slide polishing, metal film deposition and SPR measurement. SPR sensitivity parameters including FWHM, resolution and intrinsic sensitivity are analyzed to find the roughness effect of glass slide on the sensitivity of sensor chips. Experimental results show that the sensitivity of SPR biosensor is improved by making the surface glass slide smoother.

5.2 Experimental Methods

5.2.1 Glass slide polishing

To investigate the glass slides in different roughness condition, some of the slides were polished by using the Buehler Vector Grinding and Polishing Machine (Figure 5.1). Glass slides with size of 2cm × 2cm were purchased from Mivitec Co. The polishing process is divided into three steps, the pre-polishing preparation, polishing, and post-processing.
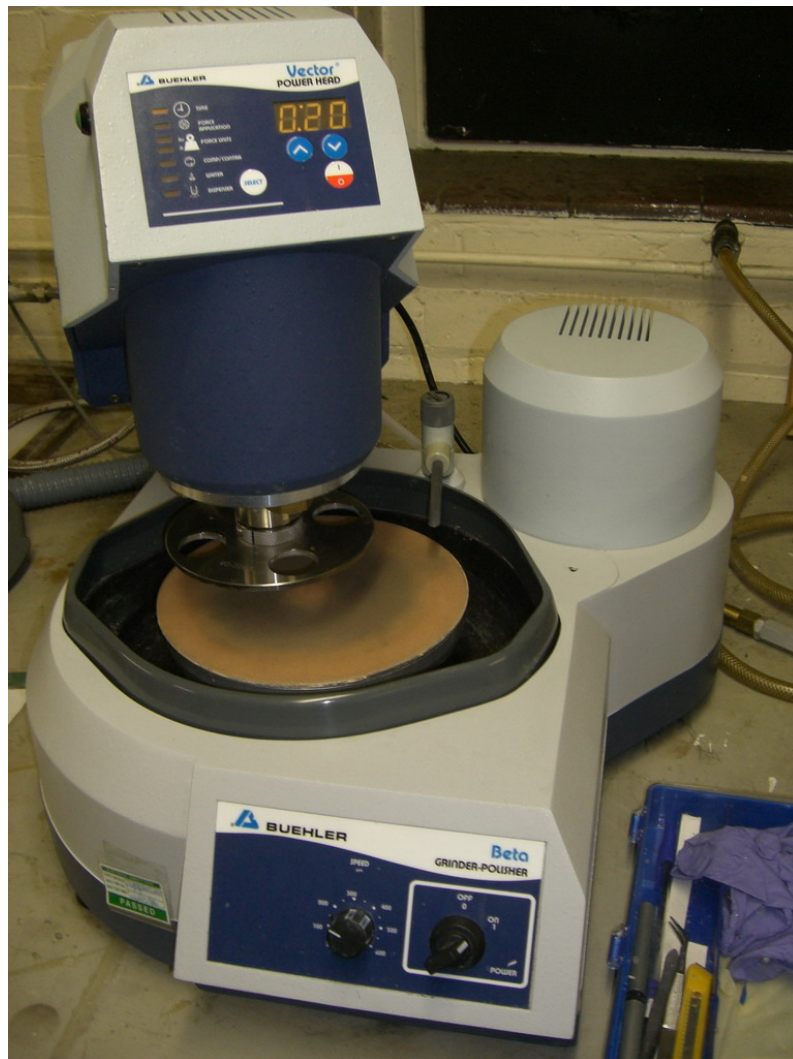
Figure 5.1 Buehler Vector Grinding and Polishing Machine

◆ **Pre-polishing preparation:**

This step was used to attach the glass slides onto a sample holder by using BPR-100

photoresist (Figure 5.2).

Figure 5.2 Sample holder

The details are:

1) Clean the glass slides with distilled water and dry them by using a nitrogen gun to

   remove dust on the surface.

2) Clean the sample holder with acetone.

3) Put a clean wafer on a hot plate at 100 degrees C for 5 minutes.

4) Leave the glass slide on the wafer and bake them for 10 minutes.

5) Put a drop of BPR-100 on the surface of glass slide. When the photoresist is heated, it is in fluid state so that it can work as an adhesive between the glass slide and the sample holder.

6) Put the sample holder on the glass slide and press it. A picture of the glass and the holder on top of a Si wafer on the hot plate is shown in figure 5.3.

**Figure 5.3** A glass slide is sandwiched by a piece of silicon wafer and the sample holder, sitting on a hot plate.

7) Cool down the sample holder for more than 10 hours. The solvent in the photoresist is evaporated completely after being left in room temperature for a long period so that the glass slide is strongly bonded to the sample holder (Figure 5.4) and is able to sustain from the force applied when the glass is polished.

Figure 5.4 Glass slides bonded on the sample holder

◆ **Glass polishing:**

The polishing process was carried out on the Buehler Vector Grinding and Polishing

Machine. First of all, a polish powder (MicroMet Cerium Oxide (CeO)-suspension,

Buehler) was diluted with distilled water and spread on the surface of polishing cloth

(MicroCloth, Buehler). Polishing results are related to the force applied, the rotating

speed and polishing time. The force applied was 4 pounds and the rotating speed of

the polishing plate was 175rpm. Glass slides were polished from 4 to 16 minutes, in

order to get different roughness values. Features of the grinding machine and its

accessories including polish powder and cloth are presented in Appendix A.

◆ Post-polishing process:

After the polishing, different particles in the polishing powder remained on the surface of glass slides. The cleaning process includes:

1) Clean the glass slide surface with distilled water to remove remaining large particles from the polishing cloth.

2) Leave the sample holder with glass slide in acetone for more than 5 hours to dissolve the BPR-100 photoresist.

3) Some photoresist remains on glass slide after it is separated from the sample holder. Clean it with acetone in ultrasonic bath for an hour to remove the photoresist.

4) Clean the glass slide with distilled water in ultrasonic bath and leave it in NaOH solution (pH<10) for 10-30 minutes. The purpose of this step is to dissolve CeO particles from the polish powder remaining on the glass slide. However, NaOH solution with high concentration can break the glass slide, therefore, a low pH was used.

◆ Roughness measurement:

The surface roughness of the polished glass slides was measured by using an interferometer. The roughness value of an entire glass slide was acquired by averaging roughness data of five areas, four on the corners and one in the middle of

glass slide.

A green light source is used in the MicroXAM interferometer (Scantron, UK). Samples are imaged by using a 50X objective lens, acquiring images in a grid array, which were subsequently stitched together. Scanning Probe Image Processor software (Image Metrology, Denmark) was employed for the analysis of the acquired images. Here are some specifications about the machine:

Vertical measurement range: 10 mm

Resolution: < 0.1 nm

RMS repeatability: approx. 0.01 nm

5.2.2 Deposition of gold film

To increase the adhesion of gold to glass, a hydrophilic surface of the glass slide is prepared. A glass slide was firstly cleaned in IPA solution ultrasonically for 10 minutes to remove dust or some particles embedded on its surface during the roughness test. Then, it was immersed in piranha solution (Concentrated Sulphuric Acid and Hydrogen Peroxide with volume ratio of 3:1) and kept on the hot plate at $80^{o}C$ for an hour to remove small organic particles. Finally, it was baked in an oven at $170^{o}C$ for at least 2 hours.

The glass slide was deposited with gold layers in a sputtering system integrated with a film thickness monitor. The sputtering system used is the BOC Edwards Auto 500 Sputtering System equipped with film thickness monitor (figure 5.5). It has high deposition rates by sputtering metal particles in a vacuum condition. During the deposition, gold particles were placed in the crucibles in the vacuum chamber and the glass slides were located on the sputtering workholder. DC power was used to sputter the gold particles onto the surface of glass slides [61, 62]. Up to four glass slides can be processed at the same time.

Figure 5.5 BOC Edwards Auto 500 Sputtering System

5.2.3 SPR measurement

SPR measurements were operated on a BIO-SUPLAR 3 SPR instrument manufactured by Analytical System from Germany (Figure 5.6). It is an angle modulation SPR instrument based on Kretschmann configuration. It is equipped with a light source and a detector, along with a prism. Water and ethanol were used as buffer solutions to change the refractive index of the sensing layer. The sensitivity parameters were obtained from the SPR curve with provided analytical software. Detailed introduction of the instrument is attached on Appendix B.
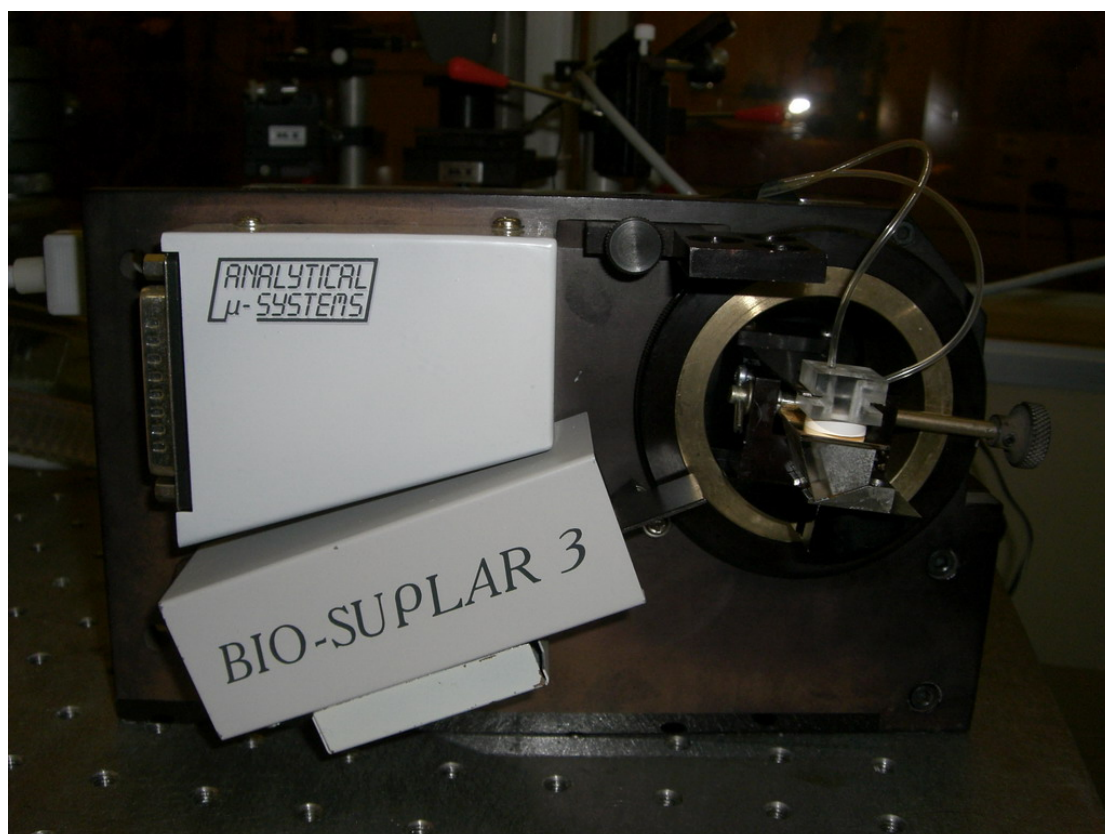

Figure 5.6 Bio-Suplar-3 SPR device.

5.3 Results and Discussion

The experimental results for polished glass slides with different surface quality are presented. Sensitivity parameters, including FWHM, resolution and IS, are analyzed and compared with simulation results.

5.3.1 Roughness measurement results

Four polished glass slides and one unpolished slide were used in the experiment. Five gold coated glass slides with different roughness condition were tested to study the roughness effects on the sensitivity of SPR biosensors. Their roughness data from interferometer are shown in the table 5.1. Ra and RMS are average value of five areas on surface of glass slides.

Table 5.1 Roughness data of selected glass slides

	Ra (nm)	Rms (nm)
Glass 1	0.6972	0.8914
Glass 2	0.6666	0.9794
Glass 3	1.506	1.898
Glass 4	1.63	2.17
Glass 5 (Unpolished)	2.565	3.23

Gold film with a thickness of 50 nm was thermally deposited on the glass slides using a BOC thermo-evaporator. The thickness value of the gold film was measured by using an Atomic Force Microscope (AFM) in tapping mode. A scratch was produced on the gold layer to make a step so that AFM can measure the film thickness (figure 5.7). As shown in figure 5.7, the minimum Z range and maximum Z range are -25 nm and 24 nm, respectively. Therefore, the total depth of gold layer is 49 nm, which is very close to the design value of 50 nm.
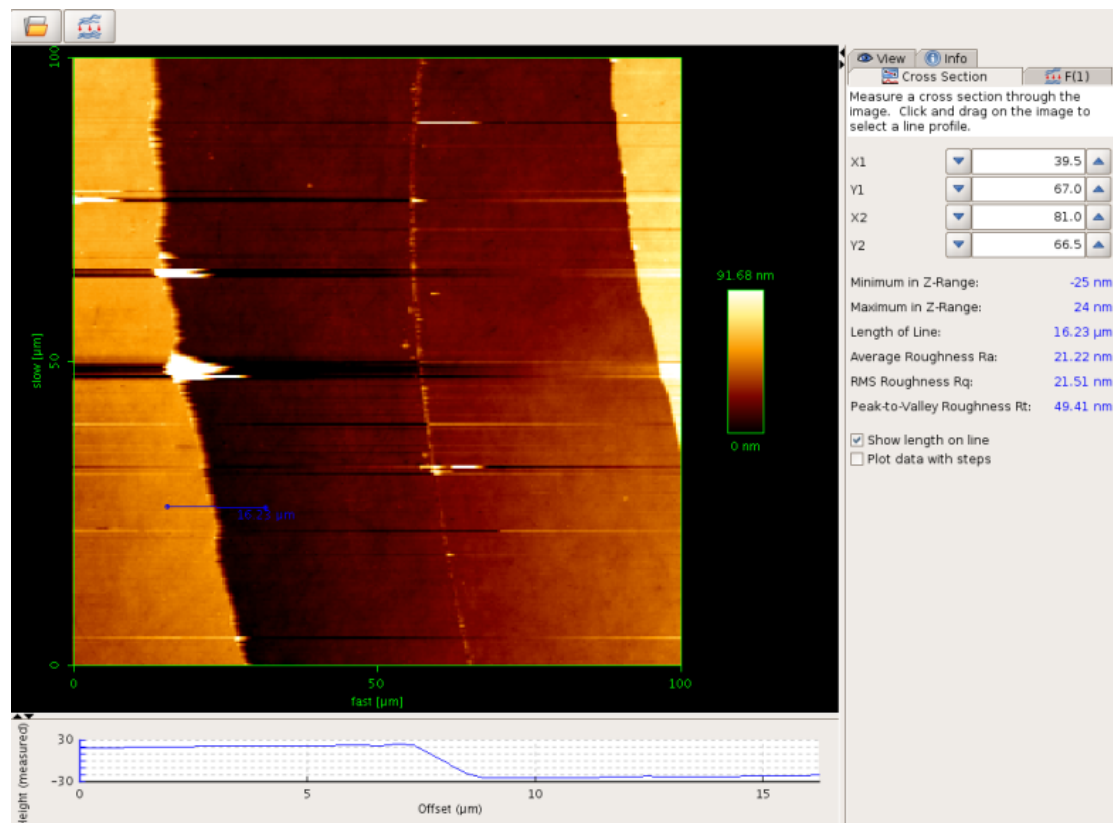

Figure 5.7 Film thickness measurement by using AFM

5.3.2 SPR measurement results

In this part, the effects of polished glass slides with different roughness values on the SPR sensitivity are analyzed in respects of several sensitivity parameters. Furthermore, the sensitivities are compared with an unpolished glass slide to reveal the improvements of sensitivity made by the polishing processes.

Figure 5.8 shows the SPR results of an unpolished glass slide on Biosuplar-3. The maximum and minimum reflectance, FWHM, and resonant angle are obtained from the image. However, the reflectance is given in reflectivity unit (R.U.). In order to compare experimental results with simulation ones, the reflectance in R.U. was changed into reflectance in percentage (%), which is used in Winspall software.
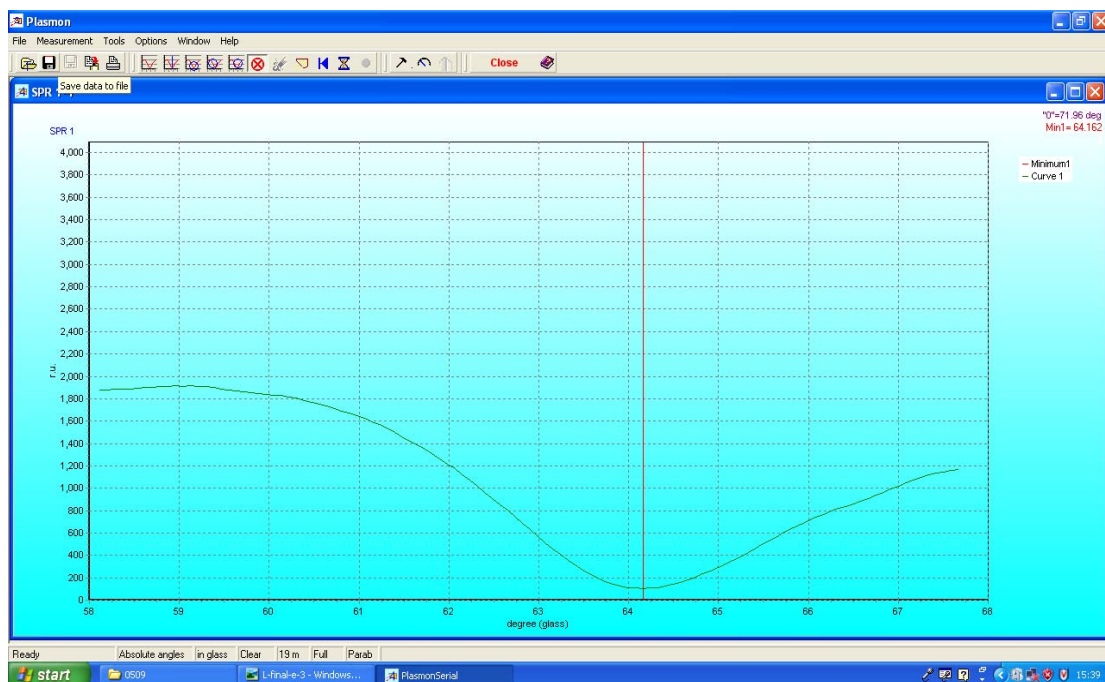

Figure 5.8 SPR curve for the gold coated unpolished glass slide

The reflectance is 100% when the incident light is completely reflected. Therefore, the reflectance unit when the incident light is completely reflected should be measured in order to transfer it into reflectance in percentage. A glass slide without metal layer was used to find out the reflectance unit for the total reflection since energy of the incident light will not be absorbed by anything on the surface of glass slide to excite surface plasmon resonance. Figure 5.9 shows that the maximum R.U. is 2580 when the total reflection happens. Therefore, reflectance in R.U. is transferred to reflectance into percentage by dividing it with 2580.
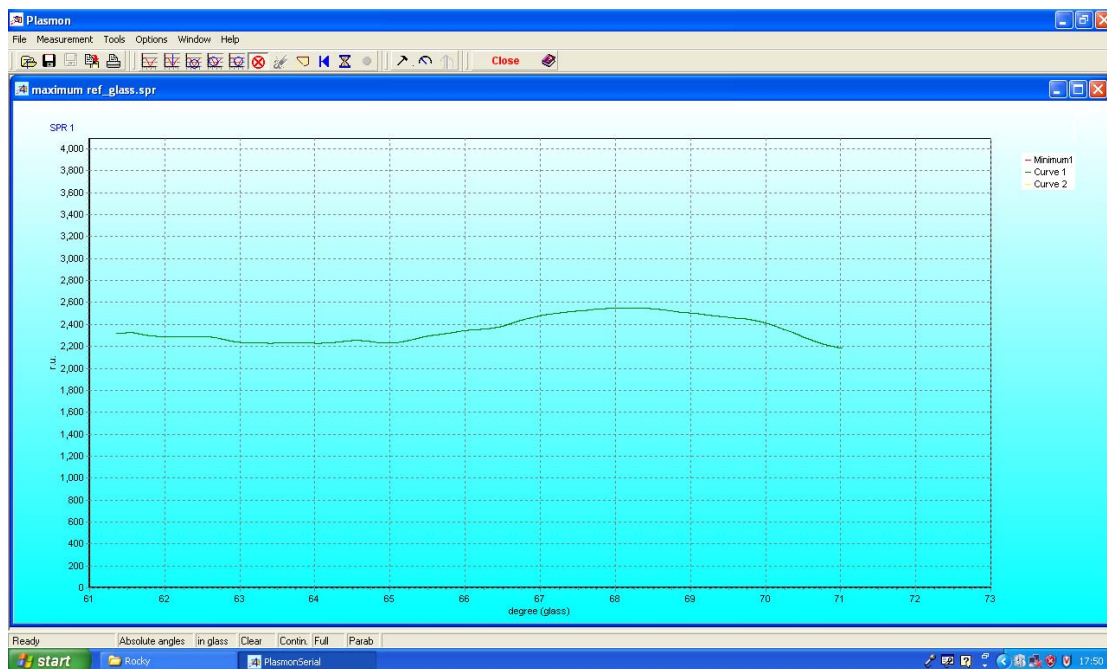

Figure 5.9 Reflectance in R.U. when total reflection happens

Now, the SPR sensitivity parameters are ready to be analyzed. As many SPR curves were obtained from experiments, they are given in Appendix C. Table 5.2 shows the

SPR sensitivity parameters based on the SPR curves. Each sample was tested on

Biosuplar-3 with water and ethanol as buffer solution for several times. The sensitivity

parameters are the averages.

Table 5.2 SPR parameters of each sample

	FWHM (degree)	Min_ref	Max_ref	Resolution (1/degree)	Angle Shift (degree)	IS
Glass 1	3.3	0.093	0.93	0.25363636	2.926	32.83950617
Glass 2	3.43	0.0871	0.744	0.19151603	3.246	35.05021056
Glass 3	3.65	0.0871	0.785	0.19120548	N/A	N/A
Glass 4	3.85	0.0349	0.988	0.24755844	3.111	29.92784993
Glass 5 (Unpolished)	4.325	0.0426	0.71	0.15431214	3.12	26.71804753

The sensitivity parameters for gold coated glass slides with different roughness

condition are plotted based on the results given in table 5.2.

◆ **FWHM**
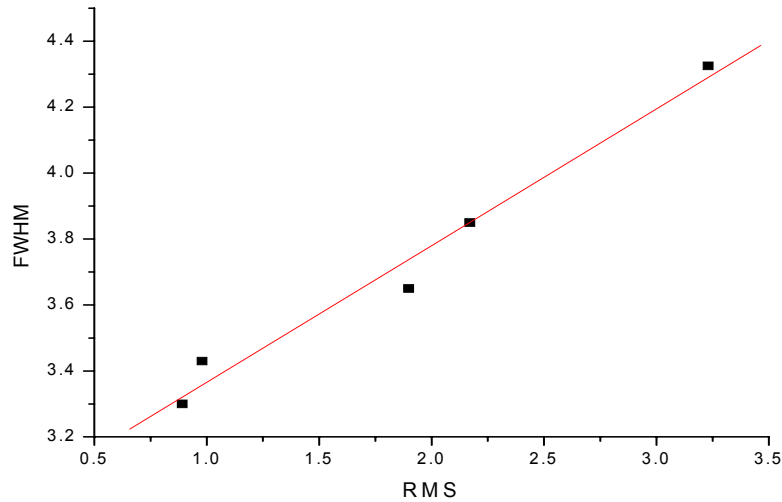
Figure 5.10 FWHM vs. RMS of glass slides.

Figure 5.10 is the linearized plot of the FWHM in response to the increasing RMS values of glass slide (Glass 1-Glass 5). The FWHM increases in proportion to the RMS values of the glass slide, which indicates that the SPR valleys become wider while the RMS values of glass slide increase, which, in turn, increases the error in determining the resonant angle from the SPR curve. The unpolished glass slide produces the largest RMS value of all. The trend of increasing FWHM in proportion to RMS values agrees with the simulation result that FWHM increases with the depth of pseudo-layer for the reason that depth of pseudo-layer $d = 2\sqrt{2}RMS$. Experimental results show that FWHM ranges from 3.2 to 4.3 degrees, while that of simulation ranges from 3.6 to 4.2 degrees. The comparison further proves the reliability of the computational work.

◆ **Resolution**
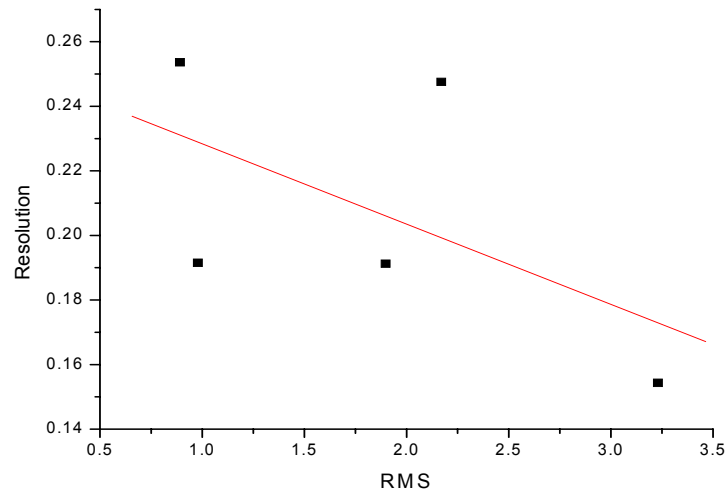
Figure 5.11 Resolution vs. RMS of glass slides (linear)

The resolution decreases with the increase of RMS of a glass slide (figure 5.11), which means the sharpness of the SPR curve decreases with the increase of RMS value. Therefore, the signal/noise ratio becomes lower and the sensitivity performance of the sensor chip gets worse with larger RMS value of glass slide. This tendency agrees with the simulation results.

◆ **Intrinsic sensitivity**
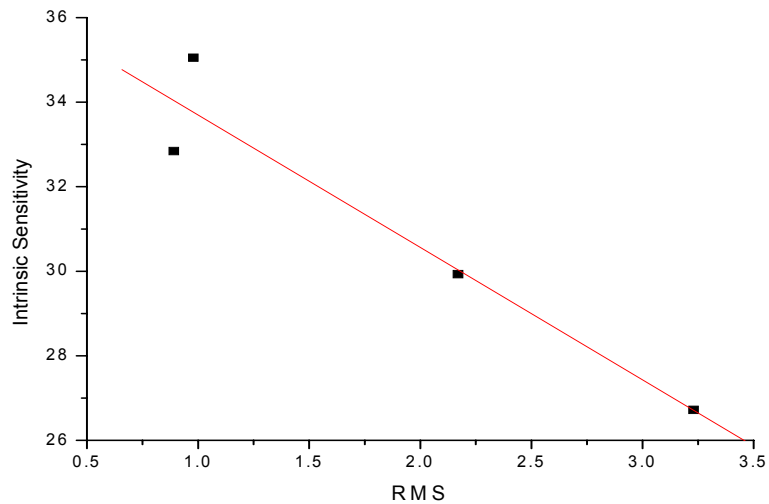
Figure 5.12 Intrinsic sensitivity vs. RMS of glass slides (linear)

Figure 5.12 shows the intrinsic sensitivity corresponding to RMS value. IS decreases with the increasing RMS value, which means that the integrated sensitivity performance of sensor chip becomes poorer with larger RMS value of glass slides. When glass 3 was measured on Biosuplar-3 with ethanol as the sensing layer, the resonant angle could not be calibrated by the equipment, therefore the resonant angle for the ethanol was not based on the same standard as that for the water as sensing layer. This resulted in the resonant angle of glass 3 not being obtained and thus the intrinsic sensitivity of glass 3. The experimental result of IS shows the same decreasing trend as shown in simulation.

5.4 Conclusions

Sensor chips have been fabricated for sensitivity improvement. Glass slides with different roughness conditions were prepared by polishing. Metal film thickness of 49 nm was well controlled in comparison with the design value of 50 nm. SPR measurement results show that FWHM increases with the RMS of glass slides while resolution decreases with it. It indicates smoother surface of glass slides produce narrower and sharper SPR curve which can reduce errors in identifying the resonant angle. At the same time it generates higher signal/noise ratio to improve the sensitivity performance of SPR sensor chip. Regarding both aspects of the narrowness of the SPR curve and the resonant angle shift, intrinsic sensitivity decreases with the increasing RMS of the glass slide. It indicates that the integrated sensitivity performance is improved by making the surface of the glass slide smoother. Experimental results agree with the simulation results. The sensitivity performance of SPR sensor chips were improved by preparing glass slides with better surface topographical quality.

6. CONCLUSIONS

6.1 Conclusions

The thesis presents the research work to improve the sensitivity of SPR sensor chips by studying bimetallic layer structure and controlling the surface roughness condition of glass slide. Computational analysis was conducted to simulate the improvements in the sensitivity of SPR sensor chips that bimetallic layer sensor chip can bring. Both simulation and experiments were conducted to investigate the effects of the surface roughness of glass on the sensitivity of SPR sensor chips. Sliver and gold coated bimetallic layer sensor chips were found effective in improving the sensitivity of current SPR sensor chips. The study on roughness effect of glass slides shows that the sensitivity of SPR sensor chips can be improved by controlling the roughness condition of glass slides.

Simulation results show that the silver gold bimetallic SPR sensors produce narrower SPR response curves than the current used SPR sensor chips with a mono gold layer. It generates almost the same narrow and sharp SPR response curves as the mono silver layer sensor chip and protects the silver layer from oxidization by coating a protective gold layer on it. An optimal combination of 45 nm thick silver and 5 nm thick gold layers was found by the simulation.

The roughness effect of glass slides was studied by introducing a pseudo-layer between the metallic layer and dielectric layer to function as the rough surface in the simulation. The simulation results show that narrow and sharp SPR curves can be produced by making a smooth surface of the glass slide. Narrow and sharp SPR curves minimize the error in determining the SPR resonant angle. Intrinsic sensitivity, which is related to both aspects of the narrowness of the SPR curve and the resonant angle shift, decreases with the depth of pseudo-layer. Both results lead to the conclusion that the sensitivity performance of SPR sensor chips can be improved by improving the surface roughness condition of the glass slides.

Sensor chips were fabricated for sensitivity improvement by polishing the glass substrates of the sensors. During the metal deposition process, metal film thickness of 49 nm was obtained comparing the design value (50 nm). The measurement results on a Biosuplar-3 SPR show that FWHM increases with the RMS of glass slides while resolution decreases with it, which indicates that smoother surface of glass slides produce narrower and sharper SPR curve and thus reduces the error in determining the resonant angle and higher signal/noise ratio as well. Intrinsic sensitivity decreases with the increasing RMS of the glass slide, indicating that the integrated sensitivity performance is improved by smoother surface of glass slide. Experimental results match the simulation results and the sensitivity performance of SPR sensor chips were improved by glass slides with better surface roughness condition.

6.2 Future work

As the optimization of the surface quality is proved to be effective in improving the sensitivity of SPR sensor chips, lots of work can be carried out in the future to produce sensor chips with better sensitivity.

First of all, materials other than silver and gold can be introduced to multi-layer system to investigate if any of these materials can further improve the sensitivity of sensor chip by using different combinations of metals.

Furthermore, efforts in controlling the surface roughness of glass slide can be made. A remarkable improvement in sensitivity of sensor chip can be generated if the glass slides are prepared as smooth as possible. More work will be involved in surface quality control and nano-scale polishing of the glass slides.

With the ever advancing technology, it is believed that in the near future, more and more SPR sensor chips with better sensitivities will be produced and put into applications.

List of References:

1. R. W. Wood, 'On a remarkable care of uneven distribution of light in a diffraction grating spectrum', *Philos. Mag. 4, pp. 396-402, 1902.*

2. R. W. Wood, 'Remarkable spectrum from a diffraction grating', *Philos. Mag. 23, pp. 310-317, 1912.*

3. U. Fano, 'The theory of anomalous diffraction gratings and of quasi-stationary waves on metallic surfaces (Sommerfield's Waves)', *J. Opt. Soc. Am. 31, pp. 213-222, 1941.*

4. A. Otto, 'Excitation of nonradiative surface plasma waves in silver by the method of frustrated total reflection', *z. Phys. 216, pp. 398, 1968.*

5. E. Kretschmann and H. Raether, 'Radiative decay of non-radiative surface plasmons excited by light', *Z. Naturforsch. 23a, pp. 2135, 1968.*

6. C. Nylander, B. Liedberg and T. Lind, 'Gas detection by means of surface plasmons resonance', *Sensors and Actuators 3, pp. 79–88, 1982.*

7. B. Liedberg, C. Nylander and I. Lundstrom, 'Surface plasmons resonance for gas detection and biosensing', *Sensors and Actuators 4, pp. 299–304, 1983.*

8. R. BM. Schasfoort and A. J. Tudos, Handbook of surface plasmon resonance, RSC Publishing, 2008.

9. E. Hecht, Optics, 4th ed., Addison-Wesley, New York, 2002

10. Z. Salamon, H.A. Macleod and G. Tollin, 'Surface plasmon resonance spectroscopy as a tool for investigating the biochemical and biophysical properties of membrane protein systems II: Applications to biological systems', *Biochim. Biophys. Acta 1331, pp. 117-129a, 1997.*

11. B. Liedberg, C. Nylander and I. Lundstrom, 'Biosensing with surface plasmon resonance—how it all started', *Biosensors Bioelectron 10, pp. i–ix, 1995.*

12. F. C. Chien and S. J. Chen, 'A sensitivity comparison of optical biosensors based on four different surface plasmon resonance modes', *Biosensors and Bioelectronics 20, pp. 633-642, 2004.*

13. P. I. Nikitin, A. A. Beloglazov, M. V. Valeiko, J. A. Creighton, J. D. Wright, 'Silicon-based surface plasmon resonance combined with surface-enhancement Raman scattering for chemical sensing', *Rev. Sci. Instrum. 68, pp. 2254-2257, 1997.*

14. P. I. Nikitin, A. N. Grigorenko, A. A. Beloglazov, M. V. Valeiko, A. I. Savchuk, O. A. Savchuk, 'Surface plasmon resonance interferometry for micro-array biosensing', *Proc. EUROSENSORS XIII, pp. 235-238, 1999.*

15. J. Homola, I. Koudela and S.S. Yee, 'Surface plasmon resonance sensors based on diffraction gratings and prism couplers: sensitivity comparison', *Sensors and Actuators B 54, pp. 16–24, 1999.*

16. J. Homola, 'On the sensitivity of surface plasmon resonance sensors with spectral interrogation', *Sensors and Actuators B 41, pp. 207–211, 1997.*

17. H. E. De Bruijn, R. P. H. Kooyman, J. Greve, 'Choice of metal and wavelength for surface-plasmon resonance sensors: some considerations'. *Appl. Opt. 31, pp. 440-442, 1992.*

18. D. Roy, 'Surface plasmon resonance spectroscopy of dielectric coated gold and silver films on supporting metal layers: reflectivity formulas in the Kretschmann formalism'. *Appl. Spectrosc. 55, pp. 1046-1052, 2001.*

19. W. B. Lin, M. Lacroix, J.M. Chovelon, N. Jaffrezic-Renault, H. Gagnaire, 'Development of a fiber-optic sensor based on surface plasmon resonance on silver film for monitoring aqueous media'. *Sens. Actuators B 75, pp. 203-209, 2001.*

20. E. M. Yeatman and E. A. Ash, 'Surface plasmon scanning microscopy', *Proc. SPIE - Int. Soc. Opt. Eng. 897, pp. 100-107, 1988.*

21. B.A. Snopok, K.V. Kostyukevich, S.I. Lysenko, P.M. Lytvyn, O.S. Lytvyn, S.V. Mamykin, S.A. Zynyo, P.E. Shepelyavyj, S.A. Kostyukevich, Y. M. Shirshov, E.F. Venger, 'Optical biosensors based on the surface plasmon resonance phenomenon: optimization of the metal layer parameters', Semiconductor Physics, *Quantum Electronics & Optoelectronics. Vol. 4, no. 1, pp. 56-69, 2001.*

22. W. Cai, H. Hofmeister, T. Rainer, 'Surface effect on the size evolution of surface plasmon resonances of Ag and Au nanoparticles dispersed within mesoporous silica', *Physica E: Low-Dimensional Systems & Nanostructures 11, pp. 339-344, 2001.*

23. P. T. Leung, D. Pollard-Knight, G. P. Malan, M. F. Finlan, 'Modeling of particle-enhanced sensitivity of the surface-plasmon-resonance biosensor', *Sens. Actuators B 22, pp. 175-180, 1994.*

24. E. Hutter, J. H. Fendler, D. Roy, 'Surface plasmon resonance studies of gold and silver nanoparticles linked to gold and silver substrates by 2-aminoethanethiol and 1,6-hexanedithiol', *J. Phys. Chem. B 105, pp. 11159-11168, 2001.*

25. L. He, M. D. Musick, S. R. Nicewarner, F. G. Salinas, S. J. Benkovic, M. J. Natan, C. D. Keating, 'Colloidal Au-enhanced surface plasmon resonance for ultrasensitive detection of DNA hybridization', *J. Am. Chem. Soc. 122, pp. 9071-9077, 2000.*

26. L. A. Lyon, M. D. Musick, M. J. Natan, 'Colloidal Au-Enhanced Surface Plasmon Resonance Immunosensing', *Anal. Chem. 70, pp. 5177-5183, 1998.*

27. F. Velge-Roussel, P. Breton, X. Guillon, F. Lescure, N. Bru, D. Bout, J. Hoebeke, 'Immunochemical characterization of antibody-coated nanoparticles', *Experientia 52, pp. 803-806, 1996.*

28. K. S. Johnston, R. C. Jorgenson, S. S. Yee, A. Russel, 'Characterization of porous sol-gel films on fiber optic surface plasmon resonance sensors', *Proc.SPIE-Int. Soc. Opt. Eng. 2068, 87-93, 1994.*

29. S. Astilean, P. Lalanne, M. Palamaru, 'Resonance-enhanced light transmission through metal nanochannels', *Proc. SPIE-Int. Soc. Opt. Eng. 4068, pp. 513-519, 2000.*

30. A. J. Haes and R. P. Van Duyne, 'A nanoscale optical biosensor: sensitivity and selectivity of an approach based on the localized surface plasmon resonance spectroscopy of triangular silver nanoparticles', *J. Am. Chem. Soc. 124, pp. 10596-10604, 2002.*

31. H. Raether, Surface plasmons on smooth and rough surfaces and on gratings, Springer, Berlin, 1988

32. R. H. Ritchie, 'Plasma Losses by Fast Electrons in Thin Film', *Physical Review vol. 106, no. 5, pp. 874–881, 1957.*

33. J. R. Reitz, F. J. Milford and R. W. Christy, Foundations of Electromagnetic Theory, Addison-Wesley, New York, 1993

34. T. Thio, 'A bright future for subwavelength light sources', *American Scientist 94, pp. 40–47, 2006.*

35. J. C. Maxwell, 'A Dynamical Theory of the Electromagnetic Field', *Philosophical Transactions of the Royal Society of London 155, pp. 459-512, 1865.*

36. K. B. Wolf, 'Geometry and dynamics in refracting systems', *European Journal of Physics 16, pp. 14-20, 1995.*

37. U. Jonsson, L. Fagerstam, B. Ivarsson, B. Johnsson, R. Karlsson, K, Lundh, S. Lofas, M. Malmqvist, H. Ostlin, B. Persson, I. Ronnberg, H. Roos, S. Sjolander, R. Stahlberg, E. Stenberg, C. Urbaniczky, 'Real-time biospecific interaction analysis using surface plasmon resonance and a sensor chip technology', *Bio Techniques 11, pp. 620-627, 1991.*

38. R. L. Rich and D. G. Myszka, 'Advances in surface plasmon resonance biosensor analysis', *Curr. Opin. Biotechnol. Vol. 11 no. 1, pp. 54-61, 2000.*

39. G. Zeder-Lutz, A. R. Neurath, M. H. Van Regenmortel, 'Kinetics of interaction between 3-hydroxyphthaloyl-beta-lactoglobulin and CD4 molecules', *Biologicals 27, pp. 29-34, 1999.*

40. T. A. Morton and D. G. Myszka, 'Kinetic analysis of macromolecular interactions using surface plasmon resonance biosensors', *Methods in Enzymology 295, pp. 268-294, 1998.*

41. A. V. Samoylov, V. M. Mirsky, Q. Hao, C. Swart, Y. M. Shirshov and O. S. Wolfbeis,

'Nanometer-thick SPR sensor for gaseous HCl', *Sensors and Actuators B 106, pp. 369-372, 2005.*

42. E. Danielan, A. Karlen, R. Karlsson, S. Winiwarter, A. Hansson, S. Löfas, H. Lennernäs and M. Hämäläinen, 'SPR biosensor studies of the direct interaction between 27 drugs and a liposome surface: correlation with fraction absorbedin humans', *J. Med. Chem. 43, pp. 2083-2086, 2000.*

43. Y. Iwasaki, T. Horiuchi and O. Niwa, 'Detection of electrochemical enzymatic reactions by surface plasmon resonance measurement', *Anal. Chem. 73, pp. 1595-1598, 2001.*

44. M. Adamczyk, P.G. Mattingly, K. Shreder and S. Yu, 'Surface plasmon resonance (SPR) as a tool for antibody conjugateanalysis', *Bioconjugate Chem 10, pp. 1032-1037, 1999.*

45. C.A. Lipschultz, Y. Li and S. Smith-Gill, 'Experimental design for analysis of complex kinetics using surface plasmon resonance', *Methods 20, pp. 310-318, 2000.*

46. V. Gaudin and P. Maris, 'Development of a biosensor based immunoassay for screening of chloramphenicol residues in milk', *Food and agricultural immunology 13, pp. 77-86, 2000.*

47. P. Englebienne, A. Van Hoonacker and M. Verhas, 'Surface plasmon resonance: principles, methods and applications in biomedical sciences', *Spectroscopy 17, pp. 255-273, 2003.*

48. R. Slavik, J. Homola, J. Ctyroky, E. Brynda, 'Novel spectral fiber optic sensor based on surface plasmon resonance', *Sens. Actuators B 74, pp. 106-111, 2001.*

49. N. A. Janunts, Sh. A. Markarian, Kh. V. Nekarayan, 'A chemo-optical sensor based on coupling of surface plasmon modes', *Sensors Actuators A 89, pp. 205-209, 2001.*

50. J. Homola, S. S. Yee, G. Gauglitz, 'Surface plasmon resonance sensors: review', *Sensors and Actuators B 54, pp. 3–15, 1999.*

51. National Communications System Technology and Standards Vision, Federal Standard 1037C, Telecommunications: Glossary of Telecommunication Terms, General Services Administration Information Technology Service,1996

52. R. Jha and A. K. Sharma, 'High-performance sensor based on surface plasmon resonance with chalcogenide prism and aluminum for detection in infrared', *Optics Letters vol. 34 no. 6, pp. 749-751, 2009.*

53. M. A. Ordal, L. L. Long, R. J. Bell, S. E. Bell, R. R. Bell, R. W. Alexander, J. Ward, C. A. Ward, 'optical properties of metals Al, Co, Cu, Au, Fe, Pb, Ni, Pd, Pt, Ag, Ti, and W in the infrared and far infrared', *Appl. Opt. 11, 1099–1119, 1983.*

54. G. J. Kovacs and G. D. Scott, 'Optical excitation of surface plasma waves in layered media', *Phys. Rev. B 16, pp. 1297-1311, 1977.*

55. E. Fontana, R. H. Pantell, 'Characterization of multilayer rough surfaces by use of surface-plasmon spectroscopy', *Phys. Rev. B (Condensed Matter) 37, pp. 3164-3182, 1988.*

56. RES-TEC, Tutorial 2 - Simulate SPR curves with WinSpall, http://www.res-tec.de/tutorial2-01.html

57. M. Cardona, 'Fresnel reflection and surface plasmon', *Am. J. Phys. 39, pp. 1277, 1971*

58. E. Kretschmann, 'The angular dependence and polarization of light emitted by surface plasmons on metal due to roughness', *Optics Communications vol. 5, no. 5, pp. 331-336, 1972.*

59. E. Kretschmann, 'Decay of non-radiative surface plasmons into light on rough silver films. Comparison of experimental and theoretical results'. *Optics Communications vol. 6, no. 2, pp. 185-187, 1972.*

60. M. Kanso, S. Cuenot and G. Louarn, 'Roughness effect on the SPR measurements for an optical fibre configuration: experimental and numerical approaches', *J. Opt. A: Pure Appl. Opt. 9, pp. 586-592, 2007.*

61. www.bocedwards.com, Auto 500 Sputtering Systems for Research and Development

62. www.bocedwards.com, Auto 500 Vacuum Coating System

APPENDIX A: POLISHING MACHINE AND ACCESSORIES

The polishing machine is Buehler Vector power head for pneumatic single force. The feature of it is listed below:

- Setting and control of time, pressure, speed and direction, automatic start and stop

- Single pressure force up to 40N per sample

- Head Speed: 60 rpm

- Choice of contra or complementary direction

The instrument includes dispenser, cable, electromagnetic water valve and control cable for Beta.

Specimen holder is made for single force to hold 4 samples with diameters of 30mm. Polishing cloth is the MicroCloth for final polishing, soft, versatile, and medium-napped synthetic. Polishing material is the MiroMet Cerium Oxide (CeO)-suspension with the particle size at 1 millimeter, usually applied to polish glass and very soft materials, being the universal polishing compound for glass.

APPENDIX B: FEATURES OF BIO-SUPLAR-3

Biosuplar-serial device includes: DC power supply (220V), Connection cord, Prism, Sample cell and Immersion liquid, together with a Biosuplar software to analyze the SPR results.

The design of the devise is presented below. It is composed of a prism mounted on the rotating drive with a corner reflector. The sensor chips are adhered to the surface of prism by using the immersion liquid between them. During the adhesion, it should be confirm that there is no air bubbles between the sensor chip and prism. After that, the sample cell, which enables the buffer solution to contact with the sensor chip surface, would be clamped up to the chip.

During the measurements, the p-polarized incident light will go through straight to the surface of the sensor chip, and will be reflected and collected by the photodiode 2, which could measure the reflected light intensity. Therefore, the resonant angle could be discovered by finding out the minimum reflectivity.
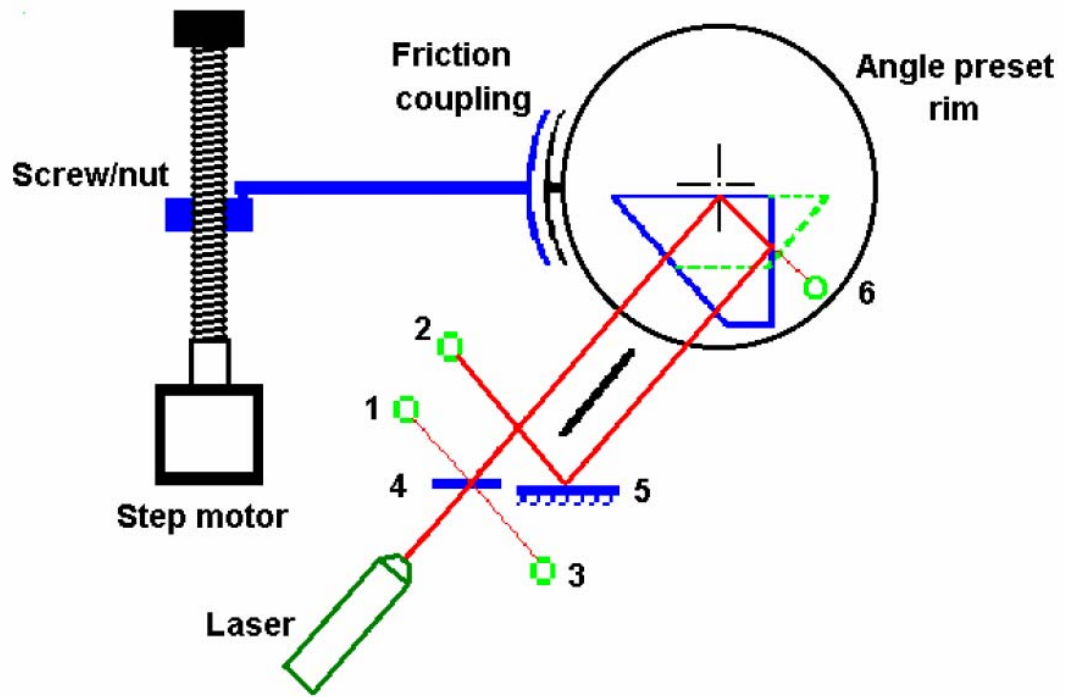
Figure B.1 Design Schematic of Biosuplar Device

APPENDIX C: SPR IMAGES OF SAMPLES WITH DIFFERENT ROUGHNESS ON

THE GLASS SLIDE
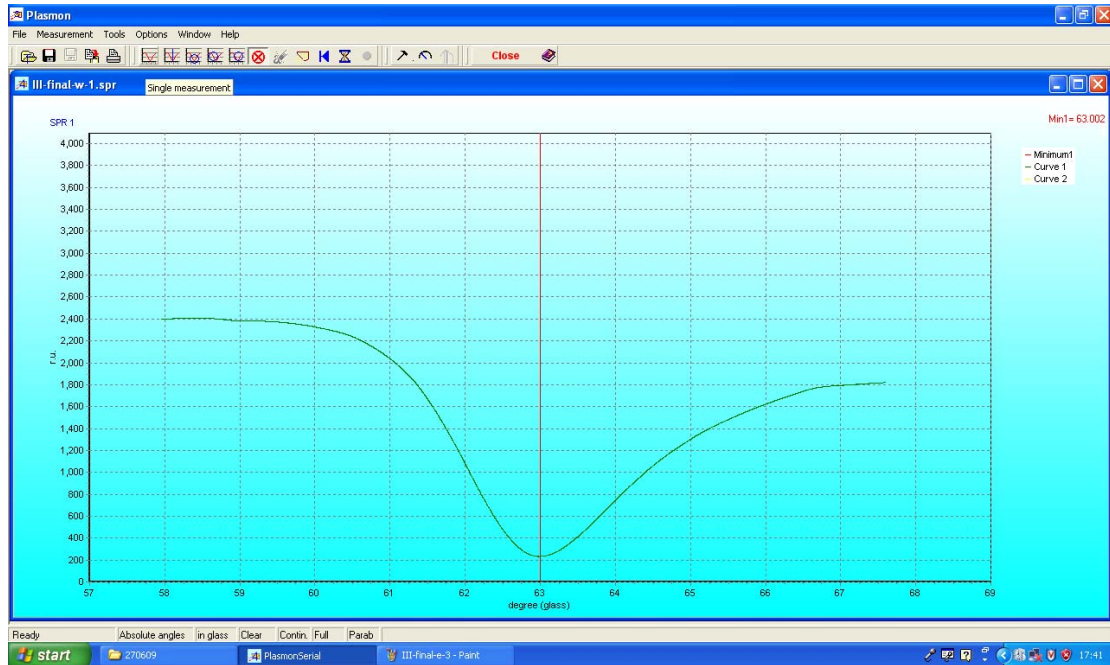
Figure C.1 SPR Curve 1 for glass 1, water as buffer solution
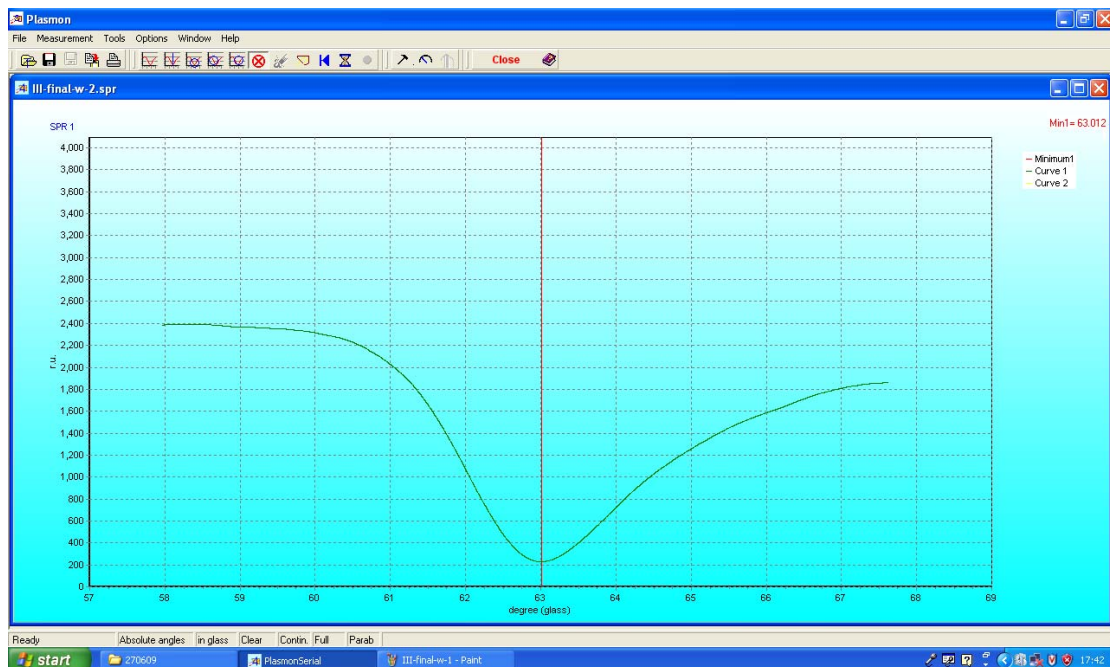
Figure C.2 SPR Curve 2 for glass 1, water as buffer solution
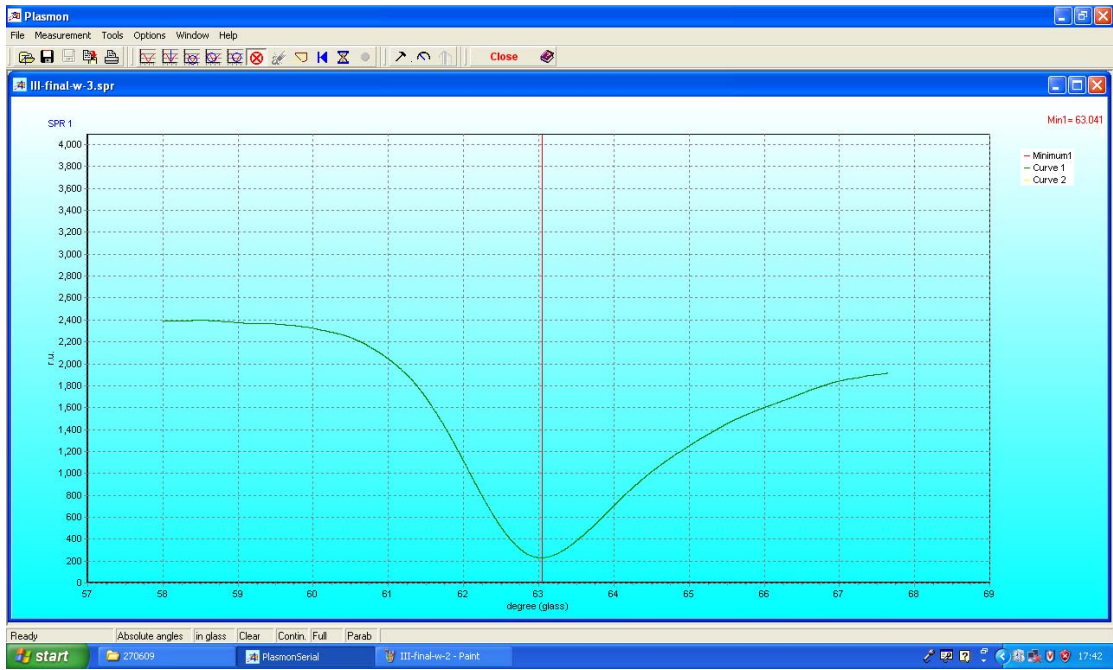
**Figure C.3** SPR Curve 3 for glass 1, water as buffer solution
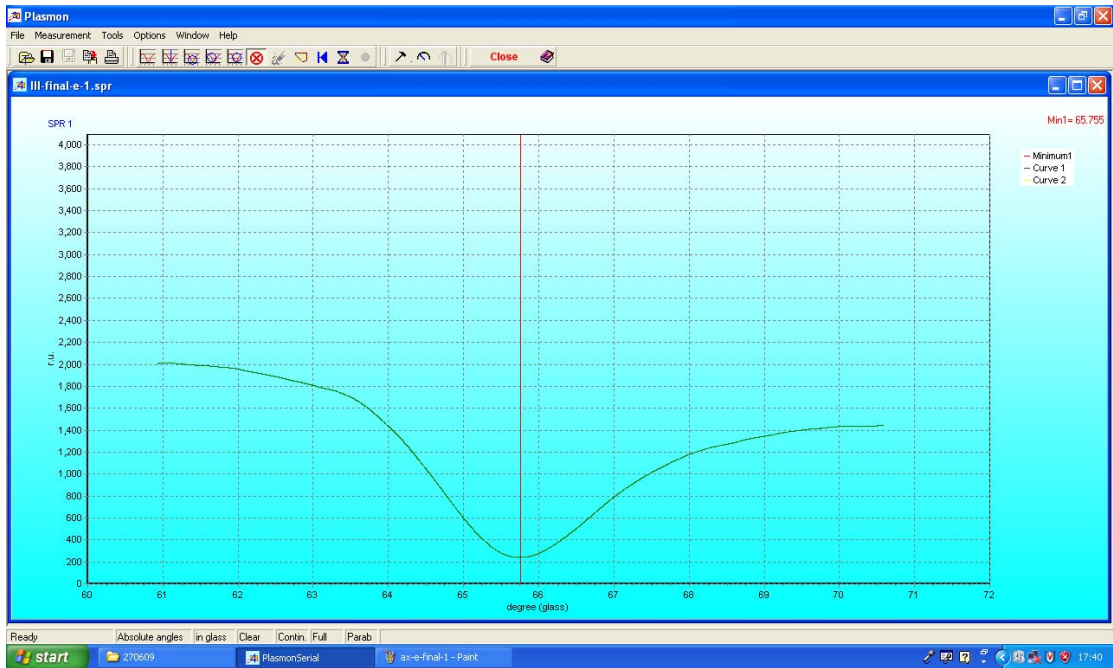
**Figure C.4** SPR Curve 4 for glass 1, ethanol as buffer solution
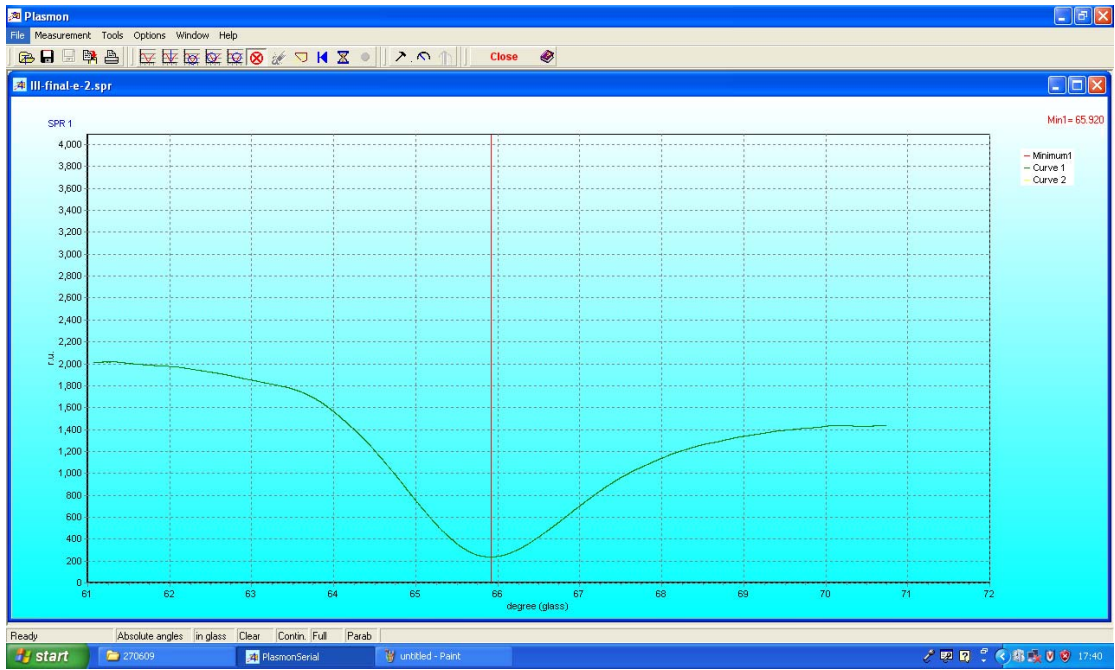
**Figure C.5** SPR Curve 5 for glass 1, ethanol as buffer solution
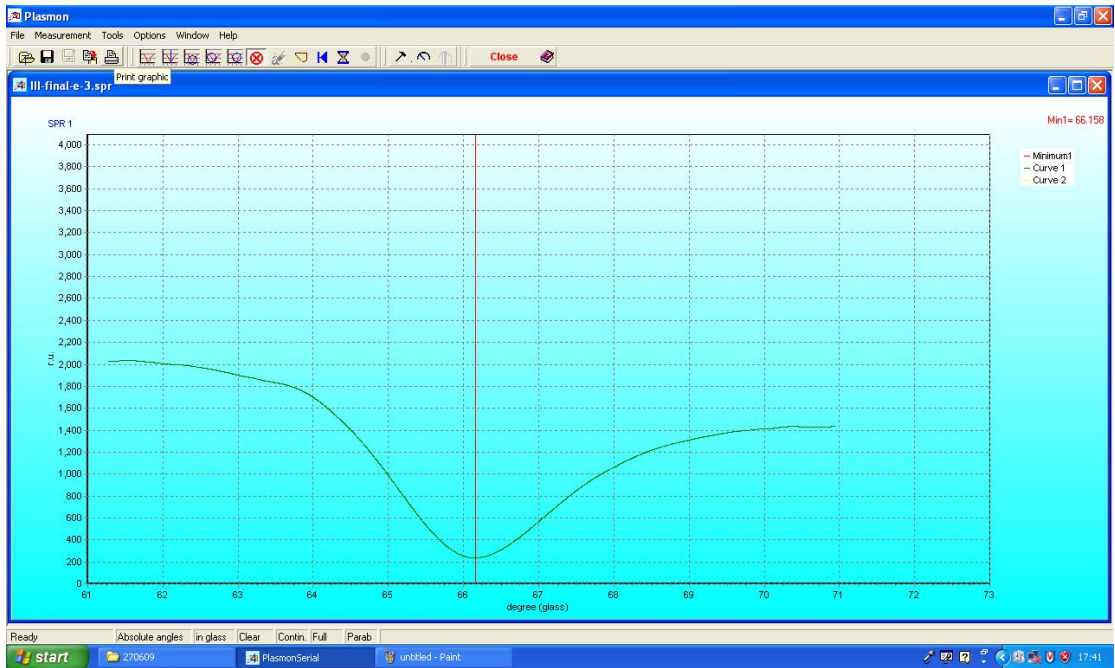
Figure C.6 SPR Curve 6 for glass 1, ethanol as buffer solution

**Figure C.7** SPR Curve 1 for glass 2, water as buffer solution
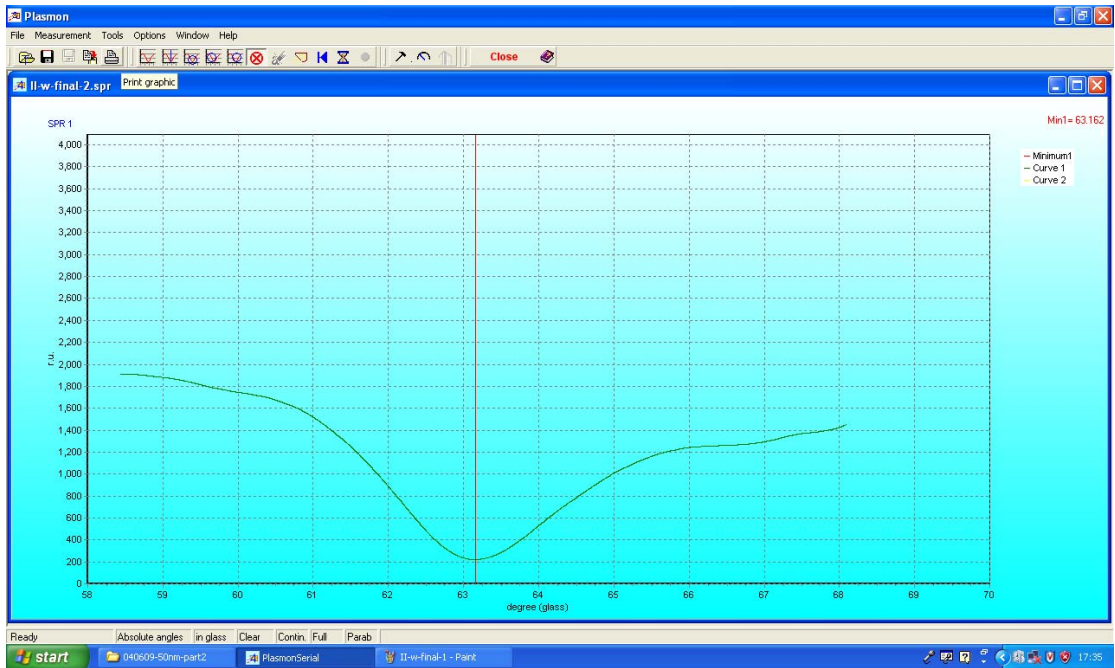
Figure C.8 SPR Curve 2 for glass 2, water as buffer solution
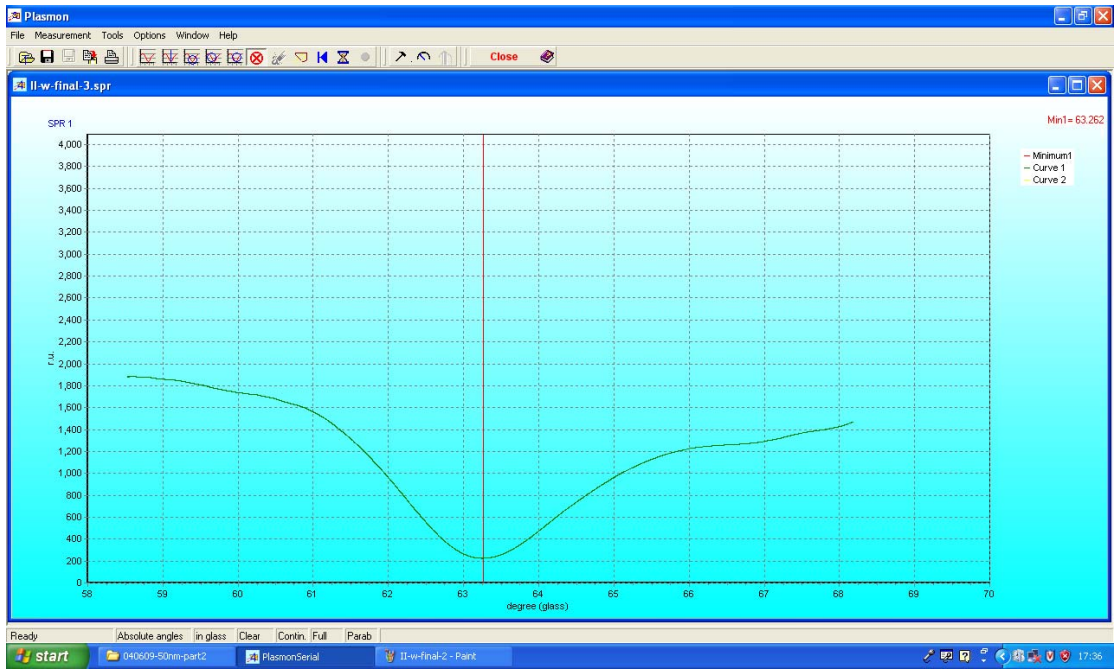
Figure C.9 SPR Curve 3 for glass 2, water as buffer solution
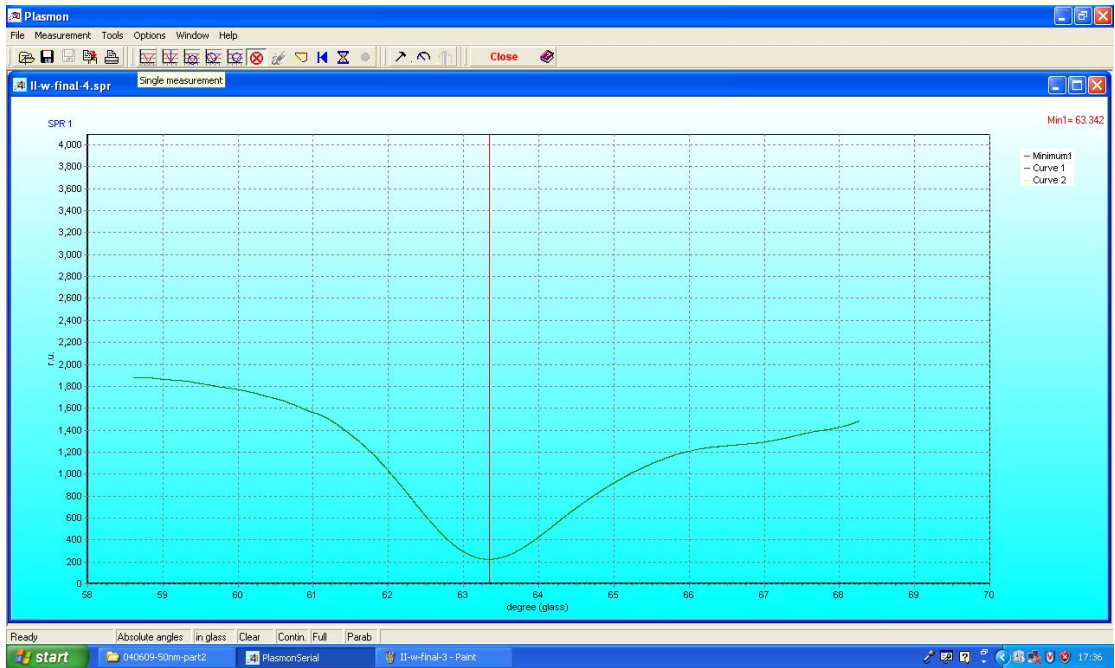
Figure C.10 SPR Curve 4 for glass 2, water as buffer solution
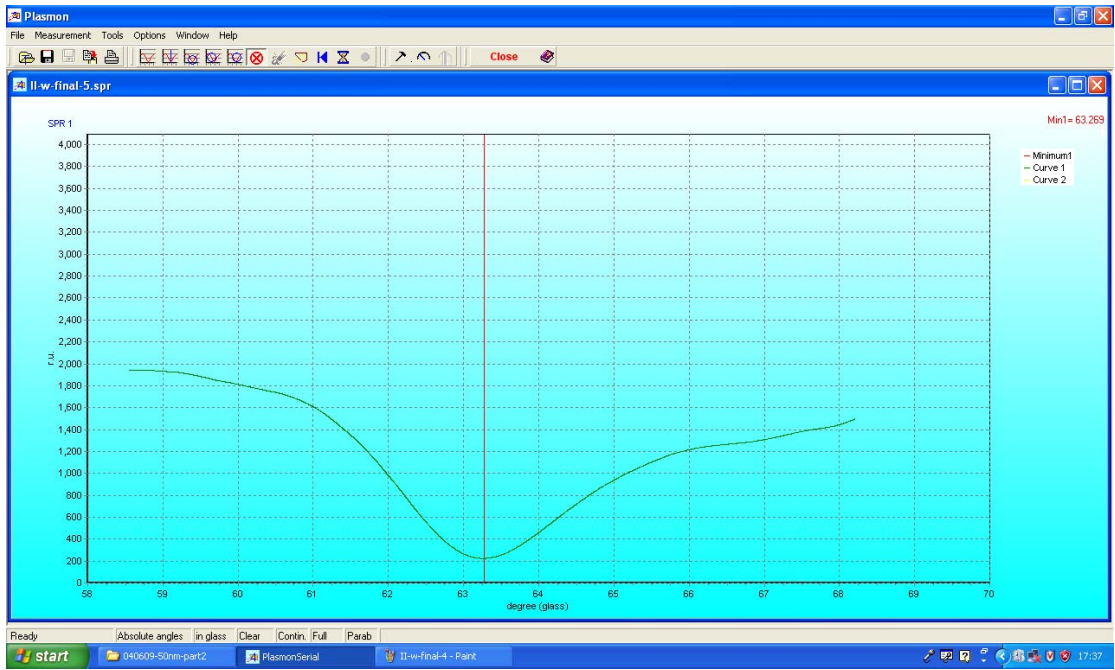
Figure C.11 SPR Curve 5 for glass 2, water as buffer solution
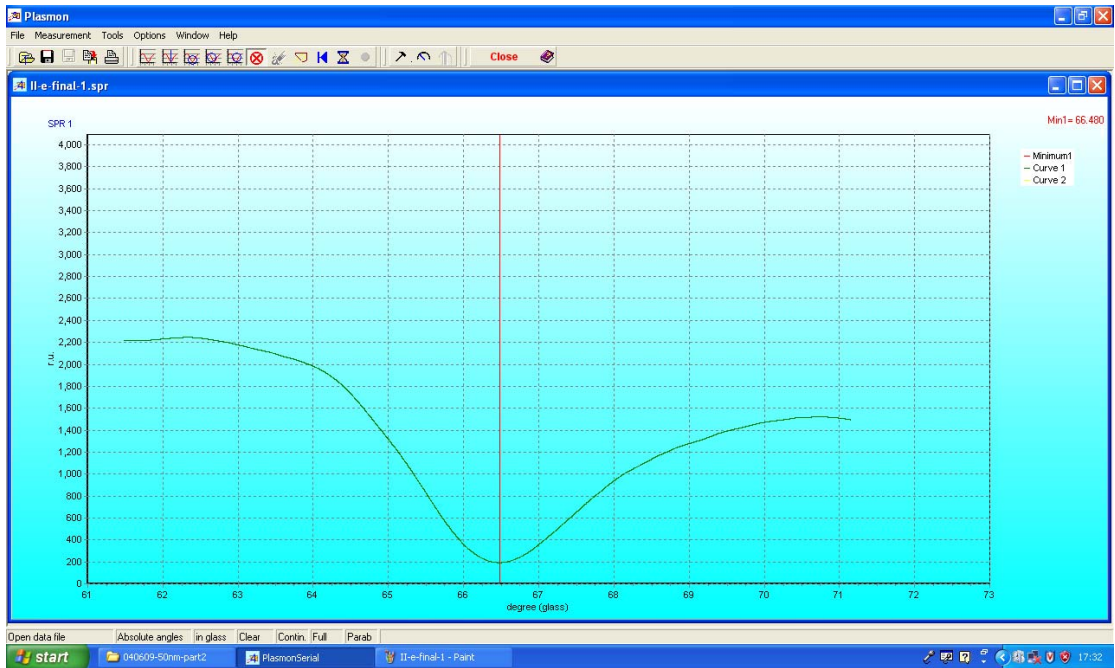
**Figure C.12** SPR Curve 6 for glass 2, ethanol as buffer solution
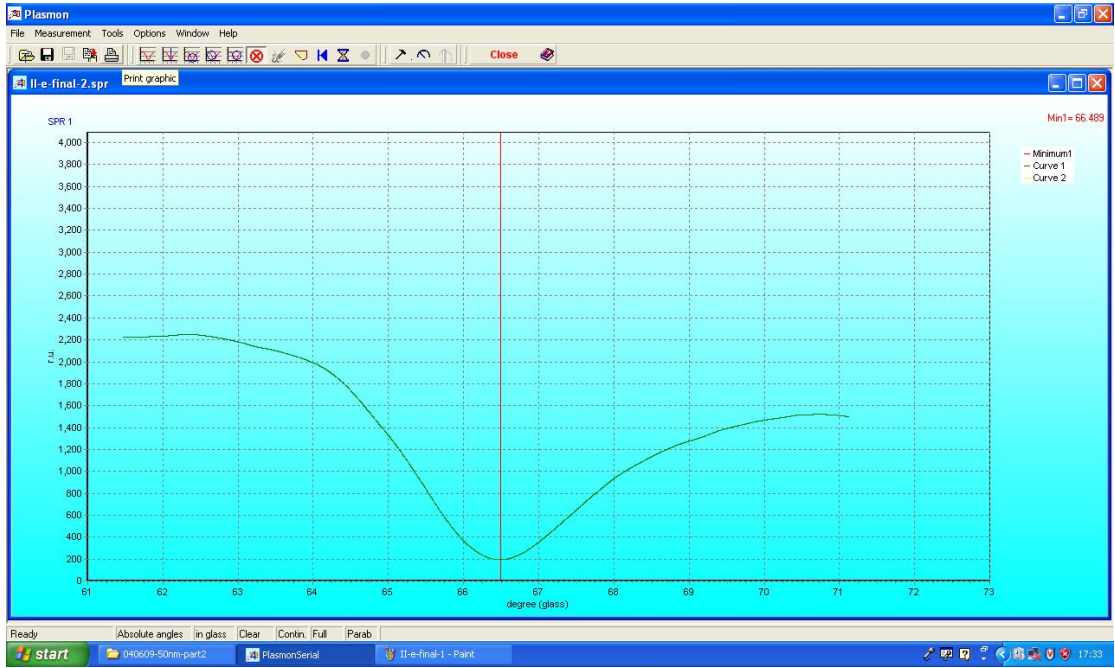
Figure C.13 SPR Curve 7 for glass 2, ethanol as buffer solution
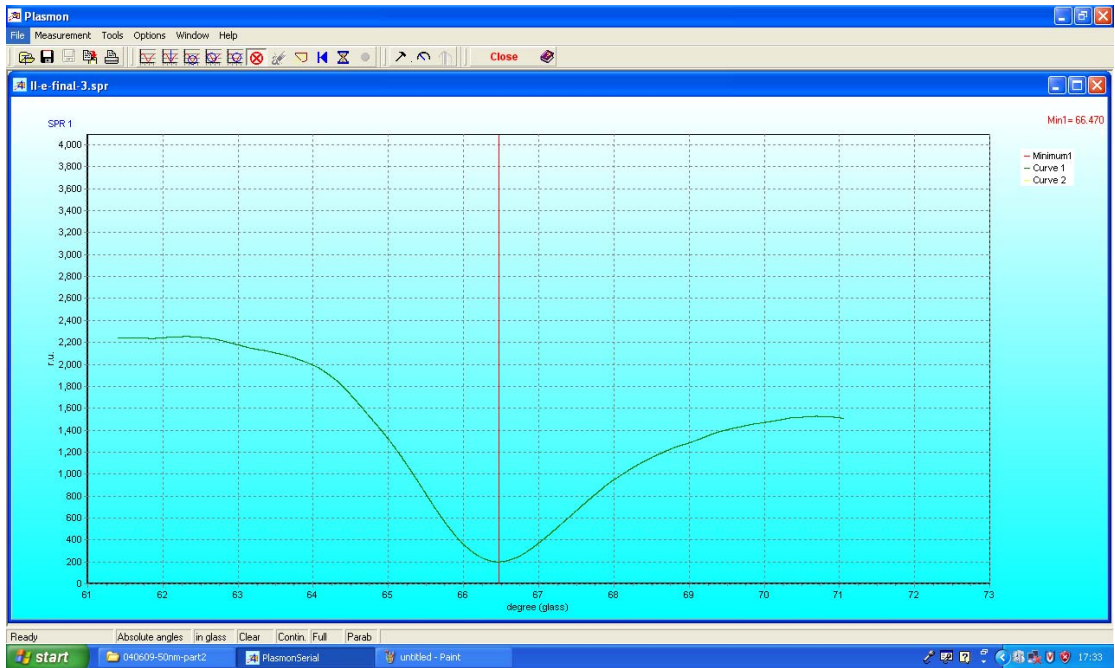
Figure C.14 SPR Curve 8 for glass 2, ethanol as buffer solution
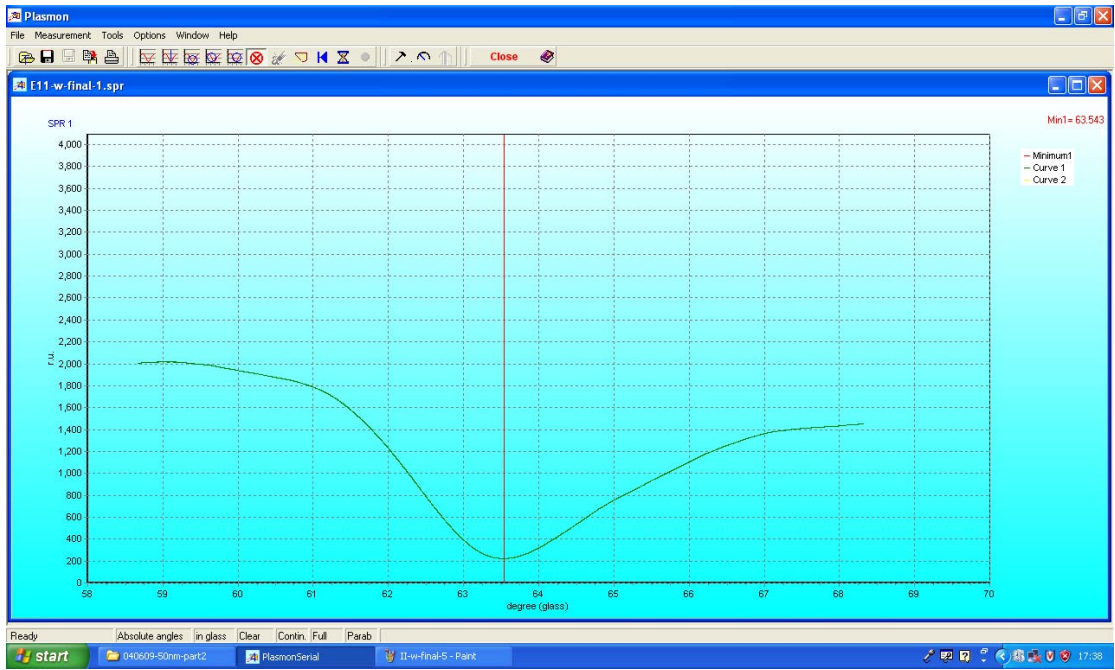
Figure C.15 SPR Curve 1 for glass 3, water as buffer solution
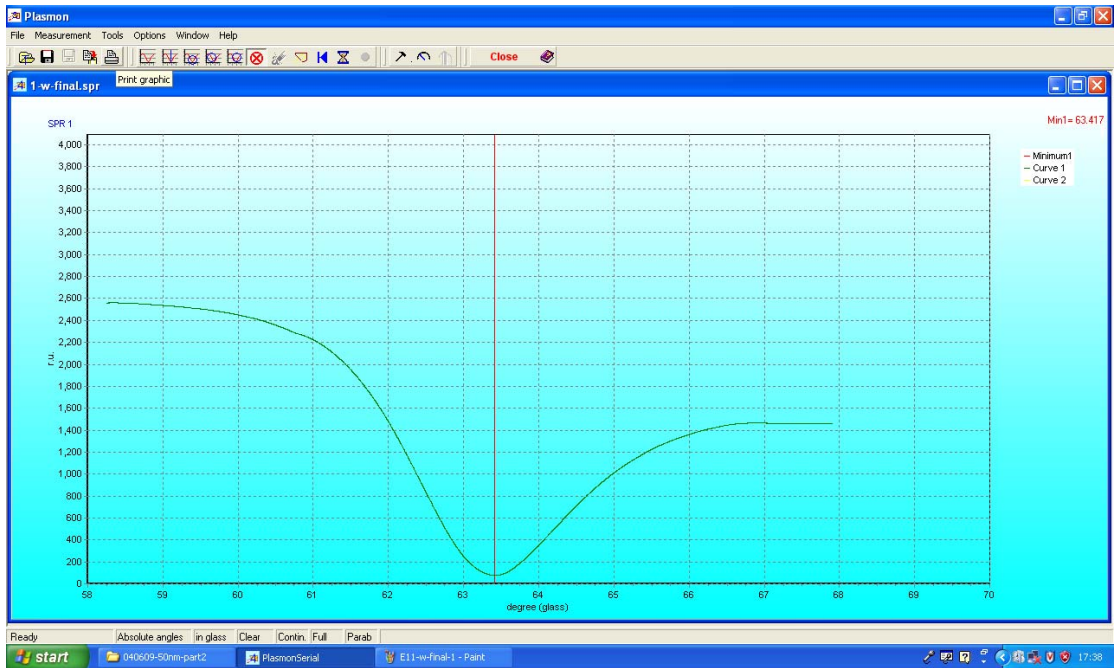
Figure C.16 SPR Curve 1 for glass 4, water as buffer solution
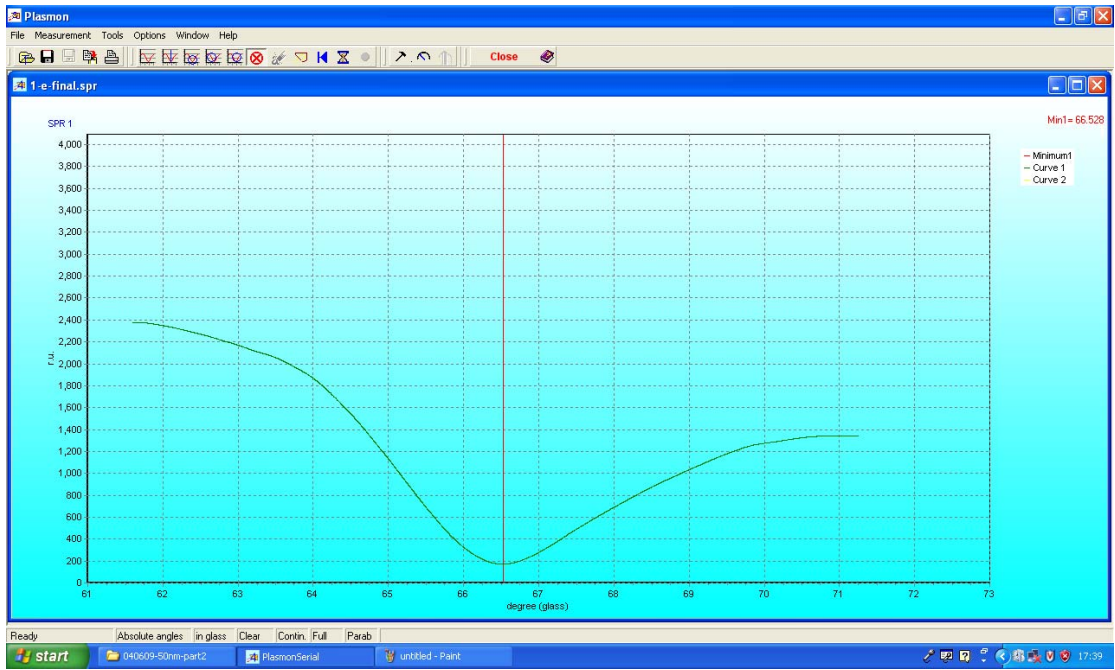
Figure C.17 SPR Curve 2 for glass 4, ethanol as buffer solution
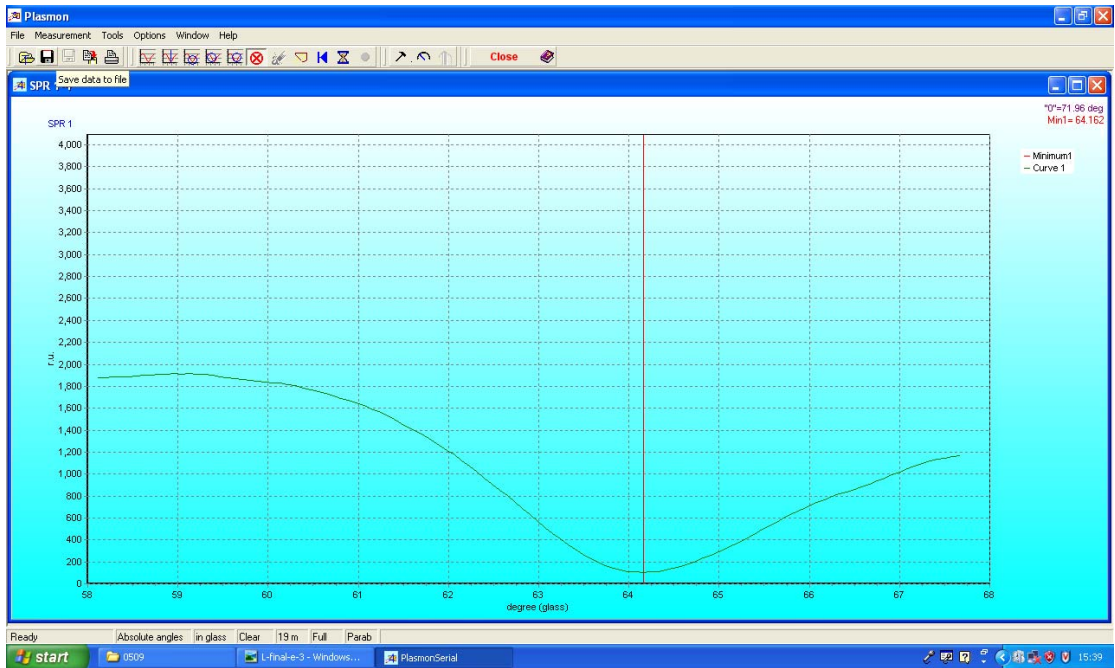
Figure C.18 SPR Curve 1 for glass 5, the unpolished one, water as buffer solution
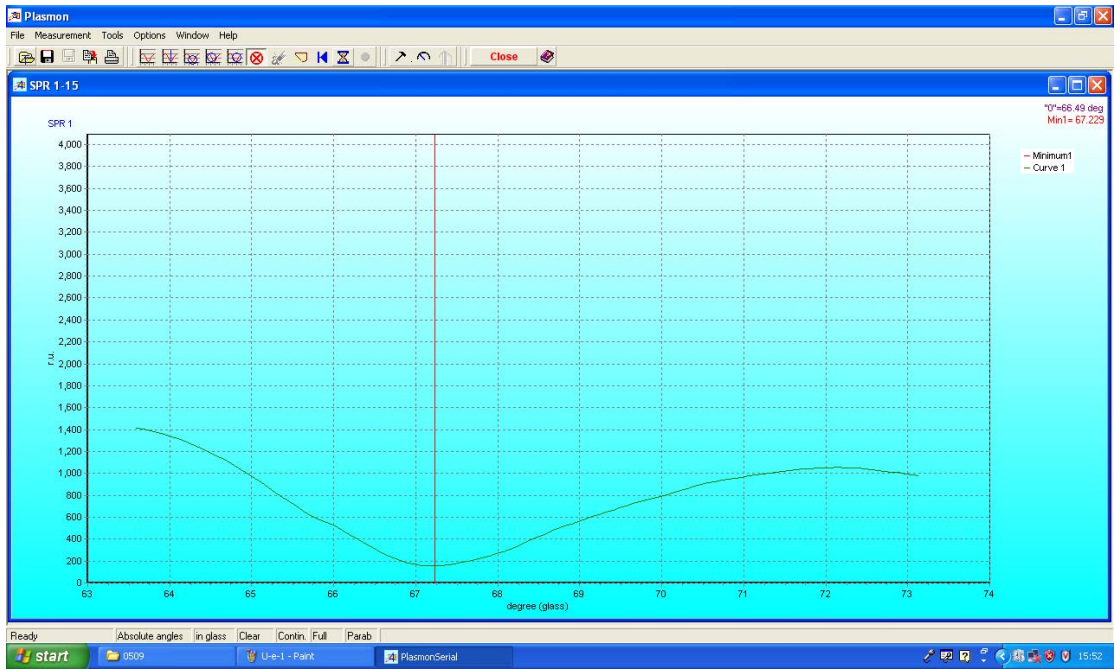
**Figure C.19** SPR Curve 2 for glass 5, the unpolished one, ethanol as buffer solution
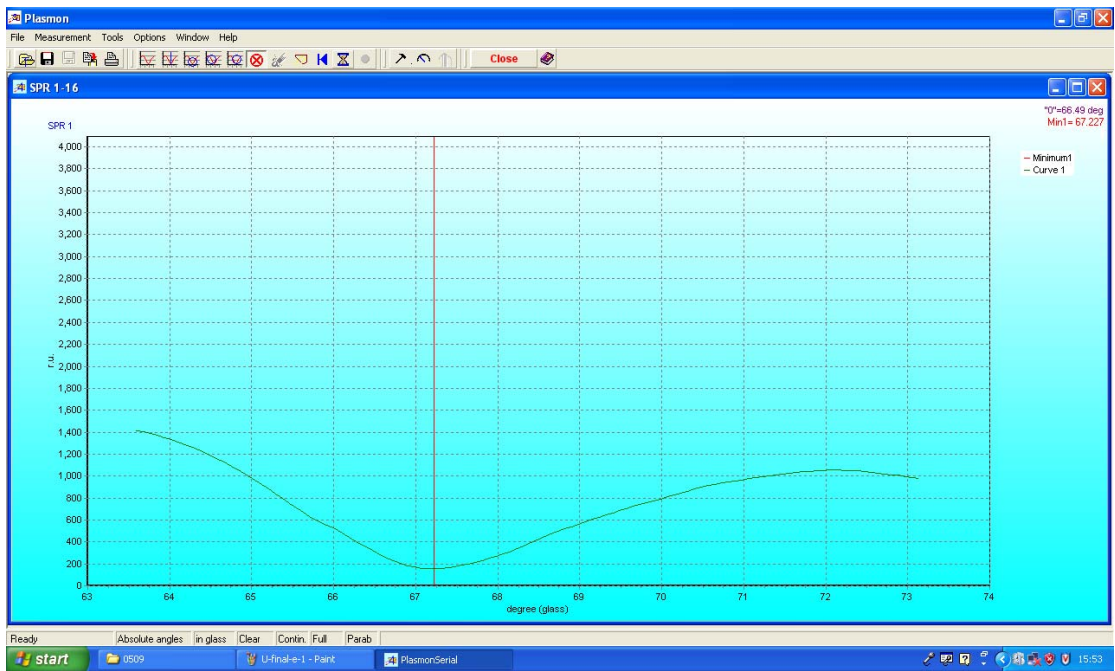
**Figure C.20** SPR Curve 3 for glass 5, the unpolished one, ethanol as buffer solution
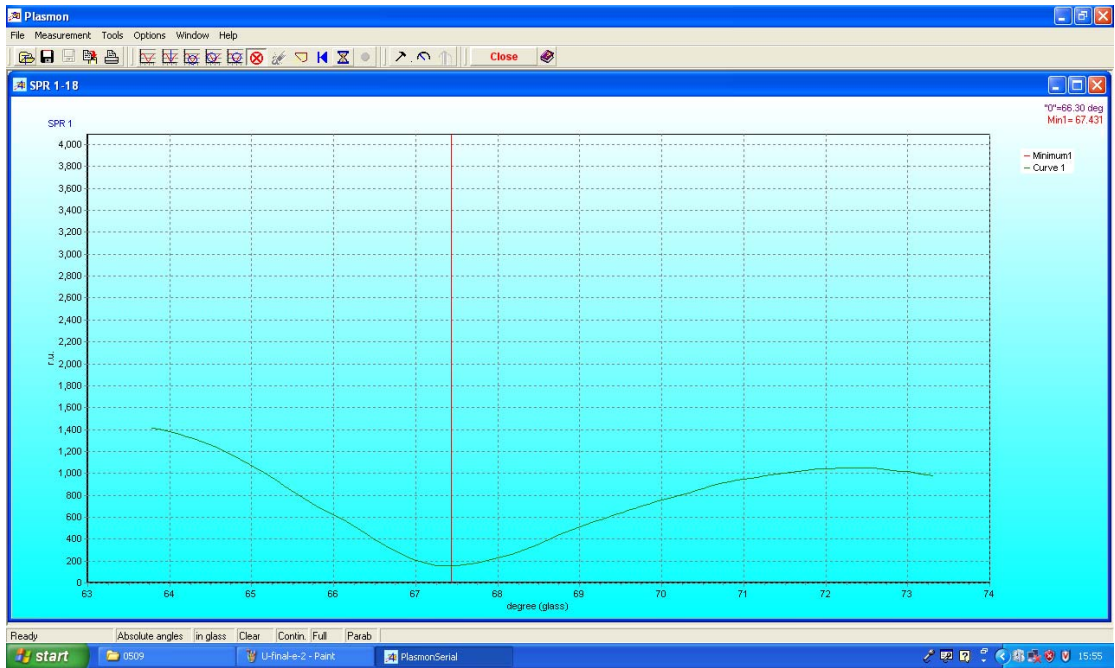
Figure C.21 SPR Curve 4 for glass 5, the unpolished one, etha nol as buffer solution
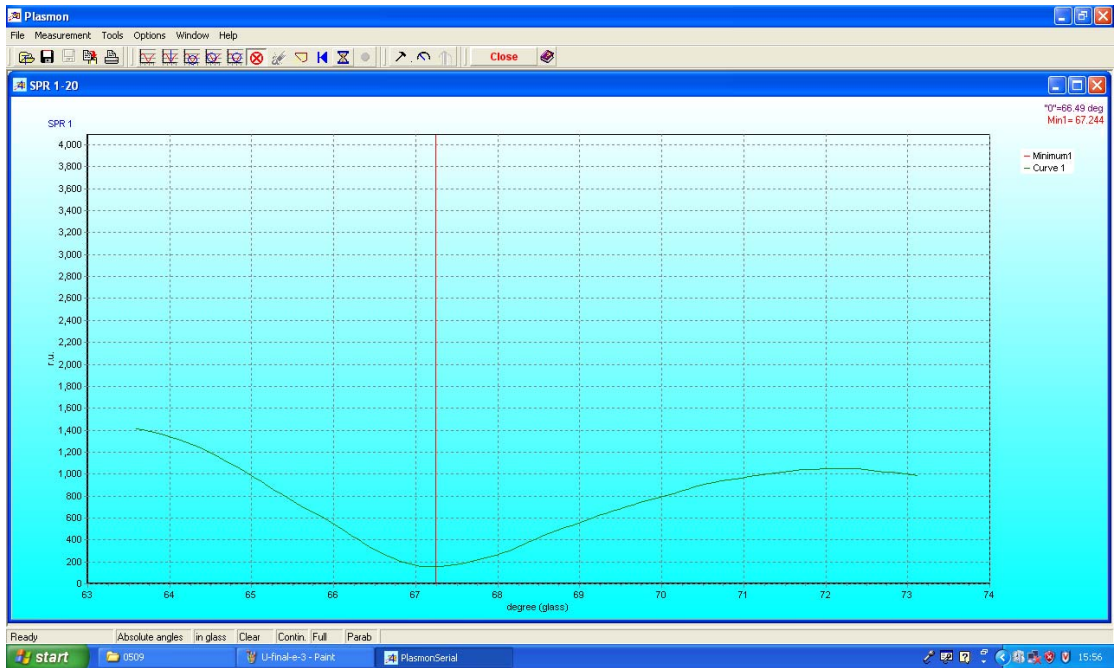

Figure C.22 SPR Curve 5 for glass 5, the unpolished one, ethanol as buffer solution